Temperature-Attributable Mortality in Elderly Brazilians: A 15-Year National Time-Series Analysis

Lucas Sempé Peter Lloyd-Sherlock

2025-12-01

1 Summary

Background Climate change is increasing temperature extremes globally. Brazil—the world's fifth most populous country—lacks national elderly-specific estimates of temperature-attributable mortality. We quantified temperature-mortality associations among elderly Brazilians (60 years) and identified vulnerable subpopulations.

Methods We analysed $13 \cdot 7$ million deaths among individuals aged 60 years across Brazil (2010–2024) using distributed lag non-linear models with two-stage meta-analysis at two spatial scales (510 immediate and 133 intermediate regions).

Findings Both heat (99th percentile) and cold (1st percentile) were associated with increased mortality. At the intermediate level: heat RR $1 \cdot 24$ (95% CI $1 \cdot 19$–$1 \cdot 29$); cold RR $1 \cdot 10$ (95% CI $1 \cdot 08$–$1 \cdot 13$); I^2=56%. We estimate 61,356 (95% CI 54,882–67,700) temperature-associated elderly deaths annually; cold-associated deaths exceeded heat-associated deaths ($2 \cdot 7$:1 ratio), reflecting cold day frequency rather than per-event lethality. The oldest-old (80+) showed highest vulnerability (heat RR $2 \cdot 04$); females showed 33% higher heat-associated mortality; cardiovascular deaths showed 84% excess on cold days.

Interpretation Non-optimal temperatures are associated with substantial elderly mortality in Brazil. Heat associations are more plausibly causal given established physiological mechanisms; cold associations may partly reflect residual seasonal confounding. Heat effects will increase under climate change, warranting prioritisation for intervention research among the oldest-old and cardiovascular patients.

Funding [To be added]

2 Research in Context

2.1 Evidence before this study

We searched PubMed and Web of Science for studies published between January 1, 2000 and November 1, 2024, using terms ("Brazil" OR "Brazilian") AND ("temperature" OR "heat" OR "cold") AND "mortality" AND ("elderly" OR "older" OR "aged"). We identified 47 relevant studies. The landmark multi-country study by Gasparrini and colleagues (2015, Lancet) included five Brazilian cities and found cold-attributable mortality ($2 \cdot 83\%$) exceeded heat-attributable mortality ($0 \cdot 70\%$)—a 4:1 ratio.[1] The seminal São Paulo study by Gouveia and colleagues (2003) first established the U-shaped temperature-mortality relationship in Brazil, with $5 \cdot 5\%$ mortality increase per 1°C below 20°C.[2] Subsequent studies confirmed cold dominance: Son and colleagues (2016) found cold effects ($8 \cdot 6\%$ excess) exceeded heat ($6 \cdot 1\%$) in São Paulo;[3] Silveira and colleagues (2019) documented this pattern across 27 cities;[4] Aschidamini and colleagues (2025) found national elderly cold effects (RR $1 \cdot 30$) exceeding heat (RR $1 \cdot 13$) in metropolitan areas.[5] The recent Latin American analysis by Kephart and colleagues (2022, Nature Medicine) confirmed temperature-mortality associations across the region.[6] The European multi-city study by Masselot and colleagues (2023, Lancet Planetary Health) found cold-attributable mortality (203,620 deaths annually) vastly exceeded heat (20,173 deaths).[7] However, existing studies had critical limitations: (1) most focused on single cities or metropolitan areas rather than true national coverage; (2) none systematically compared spatial aggregation scales to assess exposure misclassification; (3) few quantified mortality displacement (harvesting) to distinguish true excess from displaced deaths;[8] (4) none provided comprehensive elderly-specific burden estimates with 15-year follow-up.

2.2 Added value of this study

This study provides the most comprehensive national analysis of temperature-mortality associations in elderly Brazilians to date: $13 \cdot 7$ million deaths across 15 years (2010–2024). Key contributions include systematic comparison of two spatial scales showing finer resolution reduces heterogeneity (I^2 33% vs 56%); first national elderly-specific burden estimates (~61,400 annual temperature-associated deaths); clear vulnerability gradients (80+ years: doubled risk; females: 33% higher heat-associated mortality; cardiovascular deaths: 84% excess on cold days); and macro-region stratification revealing climate-adapted effect modification consistent with acclimatisation theory.

2.3 Implications of all the available evidence

Cold-associated mortality consistently exceeds heat-associated mortality in observational studies, including Brazil.[1,7,9] However, these associations should be interpreted cautiously: cold effects may partly reflect residual seasonal confounding that is difficult to fully control, and the burden estimates represent statistical associations rather than directly preventable deaths. Heat associations are more plausibly causal given event-based timing and established physiological mechanisms. Climate projections suggest heat burden will increase while cold burden may decrease,[10] reinforcing the case for heat-focused intervention research. The 80+ age group and cardiovascular patients show particularly strong associations.[11,12]

3 Introduction

Climate change is increasing the frequency and intensity of temperature extremes worldwide, with potential implications for human health.[1] Observational studies consistently demonstrate temperature-mortality associations following a characteristic J- or U-shaped pattern, with increased mortality at both cold and hot extremes.[9,12] A robust finding from global ecological research is that cold-attributable mortality substantially exceeds heat-attributable mortality in most populations—the landmark multi-country study by Gasparrini and colleagues found a 17:1 cold-to-heat ratio globally ($7 \cdot 17\%$ vs $0 \cdot 42\%$), with Brazil showing a 4:1 ratio ($2 \cdot 83\%$ vs $0 \cdot 70\%$).[1,13] Characterising these associations—while acknowledging the limitations of ecological inference—is valuable for informing public health research priorities, particularly for vulnerable elderly populations.[11]

Brazil presents a particularly important case for studying temperature-mortality associations. As the world's fifth most populous country with a rapidly ageing population (32 million elderly, 15% of population), Brazil's continental size spans tropical, subtropical, and temperate climate zones.[6,14] Existing Brazilian studies have important limitations: most focused on single cities or metropolitan areas rather than national coverage;[2–4] none systematically compared spatial aggregation scales; few quantified mortality displacement (harvesting);[8] and none focused specifically on elderly populations with comprehensive long-term national coverage.

We aimed to quantify the burden of temperature-attributable mortality among elderly Brazilians (aged 60 years) using comprehensive national data spanning 15 years (2010–2024). We applied distributed lag non-linear models (DLNM)[15,16] at two spatial scales, using nationally-defined temperature percentiles to enable cross-regional comparison (Methods), to examine: (1) the overall temperature-mortality relationship; (2) heat- and cold-attributable deaths and years of life lost; (3) mortality displacement; and (4) effect modification by age, sex, and cause of death.

4 Methods

4.1 Study design and population

We conducted a national ecological time-series analysis to quantify the association between ambient temperature and mortality among elderly Brazilians. The study period spanned 15 complete years from January 1, 2010 to December 31, 2024 (5,479 days), encompassing all registered deaths among individuals aged 60 years and older from natural causes across Brazil.

We analysed data at two complementary spatial scales defined by the Brazilian Institute of Geography and Statistics (IBGE): 510 immediate geographic regions (regiões geográficas imediatas), representing functional urban areas organised around local reference cities, and 133 intermediate regions (regiões geográficas intermediárias), which aggregate immediate regions around larger metropolitan poles.[14] This dual-scale approach allowed us to examine sensitivity to spatial aggregation and characterise the trade-off between geographic specificity and statistical stability.

Intermediate regions cover a median area of 34,629 km² (comparable to Belgium), with the median region experiencing $11 \cdot 9$ elderly deaths per day—sufficient for non-linear exposure-response estimation. Immediate regions are smaller (median 6,936 km²) with sparser mortality (median $2 \cdot 5$ deaths per day), partially explaining higher model non-convergence at this level.

The study population comprised all registered deaths among individuals aged 60 years and older from natural causes, defined as International Classification of Diseases 10th Revision (ICD-10) codes A00–R99. We excluded external causes (V01–Y98) from the primary analysis but included them in cause-specific stratification as a contrast outcome. To examine effect modification, we stratified the population by age group (60–69, 70–79, 80+ years), sex (male, female), and underlying cause of death (cardiovascular [I00–I99], respiratory [J00–J99], external [V01–Y98], and other natural causes).

This study used publicly available, de-identified administrative data from national registries and did not require ethical approval under Brazilian research regulations.

4.2 Data sources

4.2.1 Mortality data

Daily mortality counts were derived from Brazil's Mortality Information System (Sistema de Informação sobre Mortalidade, SIM), maintained by the Ministry of Health and accessible through the DATASUS public data portal. SIM is a well-established vital registration system that achieves greater than 95% coverage of deaths nationally and includes physician-certified cause of death coded according to ICD-10.[17] Coverage is highest in the South and Southeast regions (>98%) and somewhat lower in the North region (~92%), though under-registration is more common for infant and maternal deaths than elderly deaths.[17] Individual death records were aggregated to daily counts stratified by geographic region, age group, sex, and underlying cause of death.

4.2.2 Temperature data

Daily ambient temperature exposures were obtained from the ERA5 reanalysis product produced by the European Centre for Medium-Range Weather Forecasts (ECMWF). ERA5 provides hourly estimates of meteorological variables at $0 \cdot 25° \times 0 \cdot 25°$ latitude-longitude spatial resolution (~25 km at the equator) globally, derived by assimilating observational data from weather stations, radiosondes, satellites, and aircraft into a numerical weather prediction model.[18] This approach yields complete spatiotemporal coverage without missing values—a critical advantage for time-series analysis—while maintaining strong correlation with ground-based measurements ($r > 0 \cdot 95$ in validation studies against Brazilian weather stations).

We computed daily mean 2-metre air temperature as the arithmetic mean of 24 hourly values for each ERA5 grid cell. Regional temperature exposures were then calculated as population-weighted averages of all grid cells whose centroids fell within each region's boundaries, using municipality-level population distributions from the 2022 Census as weights.[14] Population weighting ensures that temperature exposures reflect conditions where elderly residents actually live, rather than uninhabited areas (forests, agricultural lands) that may comprise large proportions of region area.

4.2.3 Covariate data

To control for potential confounding by respiratory disease epidemics, we obtained weekly counts of severe acute respiratory infections (SARI) from the SIVEP-Gripe surveillance system. This allowed adjustment for influenza seasonality and the exceptional mortality disruption caused by COVID-19 during 2020–2021. However, SARI adjustment was implemented as a sensitivity analysis rather than the primary model, given potential for over-adjustment if temperature affects SARI incidence on the causal pathway to mortality.

4.3 Statistical analysis

We applied the two-stage distributed lag non-linear model (DLNM) approach that has become the methodological standard for temperature-mortality studies.[15,16,19] This framework accommodates both the non-linear relationship between temperature and mortality risk (higher risk at both cold and hot extremes) and the delayed effects of temperature exposure (mortality occurring days to weeks after exposure). The two-stage design first estimates region-specific exposure-response associations, then pools these estimates using meta-analysis to yield national summaries while properly accounting for heterogeneity.

4.3.1 First stage: Region-specific models

For each of the 510 immediate regions (or 133 intermediate regions), we fitted a quasi-Poisson generalised linear model of the form:

$$\log[\mathbb{E}(Y_{r,t})] = \alpha_r + \text{cb}(T_{r,t}; \eta) + \text{ns}(t; 8 \text{ df/year}) + \gamma \cdot \text{DOW}_t + \delta \cdot \text{Holiday}_t + \log(\text{Pop}_r)$$

where $Y_{r,t}$ denotes the daily count of elderly deaths in region r on day t; $\text{cb}(T_{r,t}; \eta)$ is a cross-basis function capturing the two-dimensional exposure-lag-response surface for temperature; $\text{ns}(t; 8 \text{ df/year})$ is a natural

cubic spline of calendar time with 8 degrees of freedom per year to flexibly control for long-term mortality trends and seasonal patterns unrelated to temperature; DOW_t and Holiday_t are indicator variables for day of week (to capture weekly mortality cycles) and national public holidays; and $\log(\text{Pop}_r)$ is an offset for the regional elderly population, effectively modelling mortality rates rather than counts.

The cross-basis function is the methodological core of DLNM, simultaneously specifying the functional form of the exposure-response relationship and the lag structure over which effects accumulate.[15] We specified:

For the **exposure-response dimension**, we used a natural cubic spline with 4 degrees of freedom, internal knots placed at the 10th, 75th, and 90th percentiles of the pooled national temperature distribution ($18 \cdot 6$°C, $26 \cdot 6$°C, and $27 \cdot 8$°C respectively), and boundary knots at 0°C and 40°C. This specification allows sufficient flexibility to capture the J-shaped or U-shaped relationship commonly observed while avoiding overfitting in temperature ranges with sparse data.

For the **lag-response dimension**, we used a natural cubic spline with 4 degrees of freedom, a maximum lag of 21 days (extended to 35 days in harvesting analyses), and internal knots placed at equal intervals on the log scale to allow greater flexibility for the more pronounced short-lag effects. The 21-day lag window is standard in temperature-mortality research, sufficient to capture most delayed cold effects while avoiding instability from very long lags.[1]

The cross-basis generates a coefficient vector η of length 16 (4×4 basis functions) along with its variance-covariance matrix, fully characterising the bivariate exposure-lag-response surface. Models were fitted using iteratively reweighted least squares with convergence defined as relative change in deviance <10 between iterations (R default). The quasi-Poisson dispersion parameter was estimated as $\hat{\phi} =$ Pearson residual deviance$/(n-p)$; median $\hat{\phi}$ across converged models was $1 \cdot 18$ (IQR $1 \cdot 08$–$1 \cdot 32$), indicating modest overdispersion adequately addressed by the quasi-Poisson specification. Regions with fewer than 500 total deaths or where the model failed to converge (typically due to sparse daily counts or insufficient temperature variation; 15 immediate and 4 intermediate regions) were excluded from the meta-analysis, representing $<2\%$ of total deaths.

We did not adjust for air pollution (PM . , ozone) in primary models because adjusting for pollution could induce collider bias if temperature affects both pollution levels and mortality through distinct pathways. However, we conducted sensitivity analyses adjusting for satellite-derived CAMS reanalysis pollution data (PM . and ozone). Pollution-adjusted estimates showed minimal change: heat RR $1 \cdot 295$ (95% CI $1 \cdot 253$–$1 \cdot 338$) versus baseline $1 \cdot 301$ ($-0 \cdot 5\%$ change); cold RR $1 \cdot 275$ (95% CI $1 \cdot 243$–$1 \cdot 308$) versus $1 \cdot 271$ ($+0 \cdot 3\%$ change). We similarly adjusted for severe acute respiratory infections (SARI) from SIVEP-Gripe surveillance to address potential confounding by influenza and other respiratory epidemics—particularly relevant for cold effects that may share seasonal patterns with infection dynamics. SARI adjustment produced no measurable change in estimates (heat and cold RR identical to baseline). A fully adjusted model including both pollution and SARI covariates yielded similar results. We acknowledge that satellite-derived pollution estimates carry measurement error and that SARI surveillance may not capture all respiratory infections; residual confounding remains possible, particularly for cold effects where seasonal infection dynamics may partially mediate or confound temperature-mortality associations.

4.3.2 Second stage: Meta-analysis

Region-specific coefficient vectors $\hat{\eta}_r$ and their variance-covariance matrices were pooled using multivariate random-effects meta-analysis with restricted maximum likelihood (REML) estimation.[19] This approach treats the full 16-dimensional coefficient vector as a multivariate outcome, preserving correlations between parameters and yielding a pooled exposure-lag-response surface $\hat{\eta}_{\text{pooled}}$ that accounts for both within-region sampling uncertainty and between-region heterogeneity.

From the pooled coefficients, we derived the cumulative exposure-response curve by summing effects across all lags, which represents the total mortality impact of a given temperature over the following 21 days. The minimum mortality temperature (MMT)—the temperature at which mortality risk is lowest—was estimated empirically by identifying the temperature value that minimised the cumulative relative risk curve, rather

than being fixed a priori.[20] This data-driven approach allows the MMT to reflect the local temperature-mortality relationship. All relative risks (RRs) were calculated with the MMT as the reference temperature.

We report temperature-mortality associations at several key percentiles of the national temperature distribution: P99 (extreme heat), P95 (moderate heat), P5 (moderate cold), and P1 (extreme cold). We chose nationally-defined rather than locally-defined percentiles to enable cross-regional comparability, aligning with the MCC collaborative network methodology.[1]

This approach has important implications for interpretation. National P99 ($28 \cdot 7$°C) represents a common summer day in Manaus but an exceptional heatwave in Porto Alegre; national P1 (~18°C) may be rare in the Amazon but common in southern winter. The *RR at a given national percentile* therefore conflates temperature extremeness with local exposure frequency—a $28 \cdot 7$°C day produces different physiological stress in acclimatised versus non-acclimatised populations.

Critically, however, the *burden estimates* integrate region-specific exposure-response curves with actual regional temperature distributions, meaning the burden calculation appropriately weights each region's contribution by its exposure frequency. Regions where national P99 is common contribute more heat-attributable deaths; regions where it is rare contribute fewer. The region-specific MMT (ranging 19–28°C across climate zones) further captures local physiological adaptation, as populations in warmer climates show higher MMT. The macro-region stratification results (Table 7) confirm this acclimatisation: heat effects are strongest in cooler southern regions unacclimatised to warmth, while cold effects are strongest in tropical regions unacclimatised to cool temperatures.

An alternative approach—using locally-defined percentiles (e.g., each region's own P99)—would better capture local extremeness but sacrifice cross-regional comparability and make burden aggregation conceptually problematic. We retained nationally-defined percentiles for RR reporting while allowing region-specific curves to drive burden estimation, balancing comparability with local relevance.

Between-region heterogeneity was quantified using Cochran's Q statistic and the I^2 statistic, with I^2 values of 25%, 50%, and 75% considered indicative of low, moderate, and high heterogeneity respectively.

4.4 Attributable burden estimation

We translated the estimated exposure-response relationships into population attributable burden using established backward-perspective methods.[21] For each day with observed temperature T_t differing from the MMT, we computed the attributable fraction:

$$AF_t = \frac{RR(T_t) - 1}{RR(T_t)}$$

where $RR(T_t)$ is the cumulative relative risk at temperature T_t compared to the MMT. The attributable number of deaths was then calculated as $AN_t = AF_t \times Y_t$, where Y_t is the observed death count on day t. Total attributable deaths were obtained by summing over all days in the study period. Heat-attributable mortality was defined as deaths on days with temperature above the $97 \cdot 5$th percentile; cold-attributable mortality as deaths on days below the $2 \cdot 5$th percentile. We also computed burden at the more extreme P99 and P1 thresholds.

Uncertainty in attributable burden estimates was quantified using Monte Carlo simulation (N=1,000).[1] We drew coefficient samples from the multivariate normal distribution $\eta \sim \mathcal{N}(\hat{\eta}_{\text{pooled}}, \hat{\Sigma}_{\text{pooled}})$, where $\hat{\Sigma}_{\text{pooled}}$ is the full 16×16 variance-covariance matrix from the second-stage meta-analysis (preserving correlations between exposure-response and lag-response parameters). For each Monte Carlo draw, we recalculated the cumulative exposure-response curve, derived attributable fractions and deaths, and obtained 95% confidence intervals from the $2 \cdot 5$th and $97 \cdot 5$th percentiles of the simulated distribution. This approach propagates uncertainty from the second-stage meta-analysis through the burden calculations but does not account for first-stage sampling variability, which is subsumed into the between-region heterogeneity term. To assess sensitivity of burden estimates to analytical choices, we computed alternative scenarios: (1) excluding COVID-19

years (2020–2021); (2) using pollution- and SARI-adjusted exposure-response curves; (3) using immediate versus intermediate spatial aggregation.

Years of life lost (YLL) were calculated by multiplying attributable deaths in each age stratum by sex- and age-specific remaining life expectancy from IBGE 2022 complete life tables:[14]

$$YLL = \sum_a AN_a \times e_a$$

where AN_a is the attributable number of deaths in age group a and e_a is the remaining life expectancy at the midpoint of that age group. The population-weighted average remaining life expectancy across the elderly age distribution was $12 \cdot 81$ years, ranging from approximately 18 years at age 60 to 8 years at age 85+.

Our YLL estimates use period life tables for the general elderly population, which likely overestimates actual remaining life expectancy for temperature-vulnerable individuals. Temperature-attributable deaths are concentrated among individuals with pre-existing cardiovascular disease, respiratory conditions, and frailty that independently reduce life expectancy. Additionally, if heat deaths are substantially displaced (harvesting), the standard YLL calculation further overestimates life-years lost.

We present unadjusted YLL estimates as an upper bound representing the maximum potential life-years at stake. Actual life-years saved per death prevented would likely be substantially lower—potentially 70% lower (~240,000 vs ~786,000 annual YLL) accounting for frailty, or approaching zero for severely frail individuals experiencing pure displacement (see Appendix for illustrative frailty-adjusted scenario). Without individual-level frailty data, we cannot determine the precise location within this range.

4.5 Harvesting analysis

A critical question for policy interpretation is whether temperature-related deaths represent true excess mortality or merely short-term displacement of deaths that would have occurred soon regardless—the phenomenon termed "harvesting" or "mortality displacement."[8,22] If temperature primarily affects already-frail individuals with days to weeks of remaining life, the public health burden is smaller than crude attributable death counts suggest.

To assess harvesting, we re-estimated DLNM models with extended maximum lags of 7, 14, 21, 28, and 35 days, comparing cumulative effects at each horizon. If temperature effects represent pure displacement, cumulative effects should diminish and potentially reverse at longer lags as the "borrowed" deaths create a subsequent mortality deficit. If effects represent true excess mortality, cumulative effects should persist or even increase at longer lags as delayed physiological consequences manifest.

We quantified mortality displacement using the harvesting ratio:

$$\text{Harvesting Ratio} = \frac{ERR_{7d} - ERR_{35d}}{ERR_{7d}}$$

where $ERR = RR - 1$ is the excess relative risk at the specified cumulative lag horizon. A positive ratio indicates mortality displacement (short-term effects exceed long-term cumulative effects, suggesting deaths were "borrowed" from the near future); a negative ratio indicates effects that increase over time (consistent with true excess mortality from delayed pathophysiological processes). A ratio near zero suggests stable effects across lag horizons.

4.6 Sensitivity analyses

We assessed the robustness of our findings through several complementary approaches.[23] First, we varied the maximum lag from 7 to 28 days to examine sensitivity to lag specification. Second, we varied degrees of freedom for the temperature spline from 3 to 5 to assess sensitivity to exposure-response flexibility. Third, we excluded the COVID-19 pandemic period (2020–2021) to ensure that exceptional pandemic mortality did

not distort temperature associations; this tests whether pandemic-year mortality patterns affected overall estimates. Fourth, we adjusted for weekly SARI counts as a time-varying confounder. Fifth, we compared results between immediate and intermediate spatial scales to assess sensitivity to geographic aggregation. Sixth, we examined heatwave effects by adding an indicator for periods of three or more consecutive days above the 95th temperature percentile, testing whether sustained heat exposure produced additional mortality beyond what the daily temperature model predicted. Seventh, we conducted period-stratified analyses comparing 2010–2019 versus 2022–2024 to assess whether the post-pandemic survivor cohort showed different temperature-mortality associations than the pre-pandemic population. Eighth, we performed leave-one-year-out (LOYO) cross-validation to assess temporal stability of estimates. Ninth, we stratified by Brazil's five macro-regions (North, Northeast, Southeast, South, Central-West) to examine geographic consistency and climate-adapted effect modification. Tenth, we examined socioeconomic gradients by stratifying regions by GDP per capita and urbanisation tertiles.

4.7 Effect modification

To identify vulnerable subpopulations, we examined effect modification by age group (60–69, 70–79, 80+ years), sex, and underlying cause of death. For each stratum, we repeated the complete two-stage DLNM analysis, yielding stratum-specific pooled exposure-response curves. Differences between strata were tested using multivariate Wald tests comparing the full coefficient vectors, with $p<0 \cdot 05$ considered statistically significant.[11,24]

4.8 Meta-regression

To explore sources of regional heterogeneity, we extended the second-stage meta-analysis to include region-level covariates as moderators using multivariate meta-regression.[25] Tested moderators included: the proportion of regional population aged 60 years and older (as a marker of demographic vulnerability), urbanisation rate (percentage of population in urban areas), regional GDP per capita (as a socioeconomic indicator), and temperature variability (standard deviation of daily temperature, as a marker of climate stability and population acclimatisation). Residual I^2 after covariate adjustment indicated the proportion of heterogeneity explained by measured moderators.

4.9 Software and reproducibility

All analyses were conducted using R version $4 \cdot 4 \cdot 1$. Primary packages included dlnm (version $2 \cdot 4 \cdot 7$) for distributed lag non-linear modelling, mixmeta (version $1 \cdot 2 \cdot 0$) for multivariate meta-analysis and meta-regression, gnm (version $1 \cdot 1 \cdot 2$) for generalised non-linear models, and sf for spatial operations.[15] Complete analysis code and intermediate results are available at [repository URL to be added upon publication].

5 Results

5.1 Study population and temperature distribution

Over the 15-year study period from January 1, 2010, to December 31, 2024, we analysed 13,677,712 deaths among Brazilians aged 60 years and older from natural causes. The study population encompassed the entirety of Brazil's elderly population, spanning all 5,570 municipalities across 27 federative units, from the equatorial Amazon basin to the subtropical southern states.

At the intermediate health region level (133 regions), 129 regions ($97 \cdot 0\%$) had sufficient data for model convergence, contributing 660,980 region-days of observation with a median of 4,970 region-days per region (interquartile range [IQR] 4,380–5,475). At the immediate health region level (510 regions), 495 regions ($97 \cdot 1\%$) converged successfully, contributing 2,302,539 region-days with a median of 4,520 region-days per region (IQR 3,650–5,110). This high convergence rate (97%) is consistent with comparable multi-region temperature-mortality studies and reflects adequate statistical power across the vast majority of Brazilian health regions.

Four intermediate and 15 immediate regions were excluded from the meta-analysis due to sparse mortality data (fewer than five deaths per day on average) or insufficient temperature variation for non-linear exposure-response estimation. These 19 excluded regions were concentrated in small, rural areas: 10 in Santa Catarina, four in Paraná, two in Acre, and one each in Rondônia, Minas Gerais, and Rio Grande do Sul (Appendix Table A3). These regions collectively represent less than 2% of the elderly population and are unlikely to materially affect national estimates; for mapping purposes, pooled national estimates were imputed to these regions (indicated by hatched areas in Figures 6–7).

Daily mean temperature across all regions ranged from $8 \cdot 2$°C to $34 \cdot 6$°C, reflecting Brazil's enormous climatic diversity from tropical equatorial to humid subtropical zones. The 1st percentile of temperature (P1, our extreme cold threshold) ranged from $18 \cdot 7$°C to $20 \cdot 2$°C across regions; the 99th percentile (P99, extreme heat threshold) was $28 \cdot 7$°C. The median daily temperature was $24 \cdot 0$°C (IQR $22 \cdot 1$–$26 \cdot 3$°C). These temperature distributions confirm that even "cold" temperatures in Brazil are moderate by global standards—the P1 threshold of 18–20°C would be considered mild in temperate European climates where cold mortality occurs at temperatures near or below 0°C.

This raises the question of whether cold-related mortality in Brazil reflects the same pathophysiological mechanisms as in temperate settings. We believe the answer is largely affirmative, based on three lines of evidence:

First, relative cold thresholds are biologically meaningful. The pathways linking cold to mortality—sympathetic activation, peripheral vasoconstriction, hypertension, increased blood viscosity, impaired mucociliary clearance—are triggered by relative rather than absolute cold, i.e., temperatures substantially below an individual's acclimatised optimum.[1,26] Laboratory studies demonstrate that thermoregulatory responses scale with deviation from individual thermal optima, not absolute temperature.[27] Brazilian elderly acclimatised to tropical temperatures of 24–28°C may experience comparable physiological stress at 18°C as European elderly acclimatised to 10–15°C experience at 0°C. This acclimatisation hypothesis is supported by the consistent finding that minimum mortality temperatures occur at roughly the 75th–80th percentile of local temperature distributions worldwide, regardless of absolute temperature levels.[1,13]

Second, cold effects are not confined to cooler southern regions. If cold mortality in Brazil merely reflected subtropical temperatures approaching biologically absolute cold thresholds, we would expect effects concentrated in southern states where temperatures genuinely approach European-style cold. Our macro-region analysis shows otherwise: while the South (mean annual temperature $18 \cdot 8$°C) shows the strongest cold associations (mean RR $1 \cdot 48$), tropical regions show substantial cold effects despite never experiencing absolute cold—the North ($26 \cdot 7$°C mean) showed mean cold RR of $1 \cdot 30$, and the Northeast ($26 \cdot 1$°C mean) showed RR $1 \cdot 23$. That populations in Manaus, where temperatures rarely fall below 20°C, nonetheless show ~30% excess mortality on their coldest days strongly supports the relative threshold hypothesis.

Third, housing and behavioural factors may amplify relative cold effects. Brazilian housing stock is designed for heat dissipation rather than cold retention, heating systems are rare, and behavioural adaptations to cold (appropriate clothing, indoor heating behaviours) may be less developed than in temperate populations. These factors could potentially amplify cold vulnerability beyond what acclimatisation alone would predict—a 5°C deviation below comfort temperatures may cause greater exposure in a poorly-insulated Brazilian home than in a heated European dwelling.[24,26]

Mean daily elderly deaths across Brazil were 2,496 (range 1,847–4,112), with clear seasonal variation: winter months (June–August) showed $8 \cdot 3$% higher mortality than summer months (December–February), consistent with cold-driven excess mortality. Total elderly deaths increased from 698,247 in 2010 to 1,124,503 in 2024, reflecting population ageing and growth of the elderly cohort.

5.2 Temperature-mortality association

The pooled exposure-response relationship derived from our two-stage DLNM analysis displayed the characteristic J-shaped (or hockey-stick) curve observed in temperate and tropical settings worldwide, with mortality risk increasing at both temperature extremes relative to the minimum mortality temperature (Figure 1).

5.2.1 Intermediate health region level (133 regions)

At the intermediate level, the estimated minimum mortality temperature (MMT) was 25 · 01°C (95% CI 24 · 2–25 · 8°C), corresponding approximately to the 75th percentile of the temperature distribution. This rightward shift of the MMT toward warmer temperatures is characteristic of tropical populations and suggests adaptation to heat exposure.[1]

Extreme heat exposure (P99, 28 · 7°C) was associated with a 23 · 8% increase in mortality risk compared to the MMT (relative risk [RR] 1 · 238, 95% CI 1 · 186–1 · 292; p<0 · 0001). The heat effect curve was steep, with mortality increasing rapidly above the MMT: at P95 (27 · 5°C), RR was 1 · 14 (95% CI 1 · 10–1 · 18), rising to 1 · 24 at P99. Above the 99th percentile, the curve continued upward but with widening confidence intervals reflecting fewer observations.

Extreme cold exposure (P1, 20 · 2°C) showed a 10 · 1% increase in mortality risk (RR 1 · 101, 95% CI 1 · 078–1 · 126; p<0 · 0001). The cold effect curve was more gradual than the heat curve but extended further: at P5 (19 · 5°C), RR was 1 · 05 (95% CI 1 · 03–1 · 07), rising progressively to 1 · 10 at P1. Moderate cold (P10–P25) showed smaller but statistically significant elevations in risk.

Heterogeneity across regions was moderate (I^2 = 55 · 6%, Cochran's Q = 4,617, df = 2,048, p<0 · 001), indicating that while the overall J-shaped pattern was consistent, the magnitude of effects varied substantially by region—an expected finding given Brazil's climatic and socioeconomic diversity that we explore further in meta-regression analyses. To convey the true range of regional effects, we computed 95% prediction intervals (PI) alongside confidence intervals. For heat effects at the intermediate level, the 95% PI was 0 · 92–1 · 66, indicating that a new region drawn from the same population would be expected to have a heat RR anywhere in this range with 95% probability. For cold effects, the 95% PI was 0 · 89–1 · 36. These wide prediction intervals underscore that while the pooled national estimate is precise, individual regions may show substantially different vulnerability profiles.

5.2.2 Immediate health region level (510 regions)

At the finer immediate health region level, results were highly consistent with the intermediate analysis, providing important validation of our findings. The MMT was 24 · 76°C (95% CI 24 · 1–25 · 4°C), within 0 · 25°C of the intermediate estimate.

Heat effects remained robust: extreme heat was associated with an 18 · 3% increase in mortality (RR 1 · 183, 95% CI 1 · 157–1 · 209; p<0 · 0001). This point estimate is 4 · 5% lower than at the intermediate level, potentially reflecting reduced Berkson error from spatial exposure assignment at finer resolution.[25] Cold effects were also consistent: RR 1 · 099 (95% CI 1 · 084–1 · 115; p<0 · 0001), representing 9 · 9% excess mortality at extreme cold temperatures.

Notably, heterogeneity was substantially lower at the immediate level (I^2 = 33 · 2%, Cochran's Q = 11,836, df = 7,904, p<0 · 001) compared to the intermediate level (I^2 = 55 · 6%). The 95% prediction intervals were correspondingly narrower: 0 · 98–1 · 43 for heat and 0 · 95–1 · 27 for cold. This reduction in heterogeneity with finer spatial resolution suggests that immediate health regions capture more homogeneous populations with respect to temperature-mortality relationships, and that some apparent heterogeneity at the intermediate level reflects aggregation of diverse sub-regions.

Table 1 presents the complete temperature-mortality associations at both spatial levels, including effects at additional temperature percentiles (P2 · 5, P5, P95, P97 · 5) and confidence intervals.

5.3 Attributable burden

The translation of relative risks into absolute burden estimates reveals the substantial public health impact of non-optimal temperatures on elderly mortality in Brazil.

Intermediate level: Using Monte Carlo simulation to propagate uncertainty (N=1,000), we estimated that 16,738 elderly deaths per year (95% CI 12,480–21,080) were attributable to heat exposure (temperatures above the MMT), and 44,618 deaths per year (95% CI 37,084–52,658) were attributable to cold exposure

(temperatures below the MMT). The total temperature-attributable mortality was 61,356 deaths annually (95% CI 54,882–67,700), equivalent to 168 temperature-related elderly deaths every day in Brazil. Cold accounted for $72 \cdot 7\%$ of the temperature-attributable burden, while heat accounted for $27 \cdot 3\%$—a ratio of $2 \cdot 67$:1.

This cold dominance in attributable burden reflects *exposure frequency*, not *per-event lethality*. Cold days (below MMT) are far more frequent than extreme heat days in Brazil's temperature distribution, so even a modest cold RR ($1 \cdot 10$) accumulates more deaths than a larger heat RR ($1 \cdot 24$) applied to fewer exposure days. Per-degree departures from the MMT, heat is substantially more dangerous: the 80+ age group shows heat RR $2 \cdot 04$ versus cold RR $1 \cdot 81$, and heat effects manifest within days while cold effects accumulate over weeks. This distinction is critical for policy interpretation—the burden estimates should not be read as implying cold is inherently more dangerous than heat or that cold interventions should take priority.

Over the complete 15-year study period, this translates to an estimated 893,638 cumulative temperature-attributable elderly deaths (245,024 from heat; 648,614 from cold). To contextualise this burden: the number of deaths associated with temperature exposure exceeds those from diabetes mellitus, chronic respiratory diseases, or motor vehicle accidents over the study period.

Immediate level: Annual estimates at the immediate level were similar: 18,711 heat-attributable deaths (95% CI 15,429–21,928) and 38,121 cold-attributable deaths (95% CI 32,905–43,021), totalling 56,832 temperature-attributable deaths per year (95% CI 51,486–61,736). Cold accounted for $67 \cdot 1\%$ of the burden at this level. The modest differences between levels reflect the slightly attenuated point estimates at finer spatial resolution and different temperature exposure distributions across the regional aggregations.

5.3.1 Attributable fractions

The attributable fraction (AF) expresses the proportion of all elderly deaths that can be attributed to non-optimal temperature exposure.

At the intermediate level, the total attributable fraction was $6 \cdot 53\%$ (95% CI $5 \cdot 84$–$7 \cdot 22\%$), meaning that approximately one in every 15 elderly deaths in Brazil is attributable to temperature. The heat-attributable fraction was $1 \cdot 79\%$ (95% CI $1 \cdot 59$–$2 \cdot 00\%$), and the cold-attributable fraction was $4 \cdot 74\%$ (95% CI $4 \cdot 25$–$5 \cdot 23\%$). The cold AF was $2 \cdot 6$ times larger than the heat AF.

At the immediate level, the total AF was $5 \cdot 13\%$ (95% CI $4 \cdot 57$–$5 \cdot 69\%$), with heat contributing $1 \cdot 69\%$ (95% CI $1 \cdot 49$–$1 \cdot 88\%$) and cold contributing $3 \cdot 44\%$ (95% CI $3 \cdot 08$–$3 \cdot 80\%$). These fractions are consistent with global estimates from the Multi-Country Multi-City Collaborative Research Network, which found temperature-attributable mortality fractions of 5–9% across participating countries.[1]

5.3.2 Years of life lost

Temperature-attributable mortality translates into substantial loss of remaining life expectancy. Using age-specific life expectancy from IBGE 2022 life tables, we calculated that temperature exposure accounts for 784,685 years of life lost (YLL) annually at the intermediate level (95% CI 702,847–866,523). Heat contributed 215,151 YLL annually ($27 \cdot 4\%$), while cold contributed 569,534 YLL ($72 \cdot 6\%$).

The YLL rate was 2,443 per 100,000 elderly population per year. Each temperature-attributable death resulted in an average of $12 \cdot 81$ years of remaining life expectancy lost (range $8 \cdot 2$–$18 \cdot 4$ years depending on age at death), indicating that temperature-related deaths occur across the full elderly age spectrum, not solely among the very old.

These YLL estimates represent upper bounds; temperature-vulnerable individuals likely have shorter remaining life expectancy due to frailty and comorbidity (see Appendix for frailty-adjusted scenario).

5.4 Mortality displacement (harvesting)

We assessed whether temperature deaths represent true excess or displacement of imminent deaths by comparing effects at extended lags (7–35 days). Heat effects attenuated substantially at longer lags (RR $1 \cdot 49$

at 7 days → 1 · 00 at 35 days), a pattern consistent with near-complete displacement—though extreme heterogeneity (I^2 = 98–99%) precludes reliable quantification as this pattern varies dramatically across regions. Cold extended-lag estimates showed implausible patterns and are not interpretable. These exploratory results are hypothesis-generating only and cannot definitively distinguish true excess from displaced mortality; even displaced deaths involve suffering and healthcare burden. Full details in Appendix Table A4 and Appendix Figure A4.

5.5 Vulnerable subpopulations

Clear vulnerability gradients emerged by age, sex, and cause of death (Table 3).

Age: The oldest-old (80+) showed the highest vulnerability: heat RR 2 · 04 (95% CI 1 · 80–2 · 31), cold RR 1 · 81 (95% CI 1 · 69–1 · 94)—more than doubling mortality risk on extreme temperature days. The 70–79 group showed intermediate effects (heat RR 1 · 42, cold RR 1 · 41), and the 60–69 group the lowest (heat RR 1 · 23, cold RR 1 · 38). The 80+ group showed 66% higher heat risk than the 60–69 group (p<0 · 001).

Sex: Females showed 33% higher heat vulnerability than males (RR 1 · 94 vs 1 · 46; p<0 · 001). Cold effects showed no significant sex difference.

Cause of death: Cardiovascular deaths showed the highest cold vulnerability (RR 1 · 84, 95% CI 1 · 70–1 · 99)—84% excess mortality on cold days—consistent with cold-induced vasoconstriction, hypertension, and thrombosis. Respiratory deaths showed elevated effects for both extremes (heat RR 1 · 63, cold RR 1 · 42). External causes showed modest temperature associations (RR ∼1 · 15), which may reflect genuine mechanisms (heat impairing cognition, cold increasing fall risk) rather than pure confounding.

5.6 Regional heterogeneity

Macro-region stratification revealed climate-adapted vulnerability (Table 4): heat effects were strongest in cooler southern regions (South RR 1 · 67; Southeast RR 1 · 37) and absent in tropical regions (North RR 0 · 94; Northeast RR 0 · 96). Conversely, cold effects were strongest in tropical regions (Northeast RR 1 · 36) and minimal in the South (RR 0 · 96). This pattern—populations showing vulnerability to temperatures opposite their climate—is consistent with acclimatisation theory. Meta-regression identified temperature variability and elderly population proportion as significant moderators (Appendix).

5.7 Sensitivity analyses

We conducted extensive sensitivity analyses (detailed in Table 6). **Confounding adjustment:** Pollution-adjusted models (PM . and ozone from CAMS satellite reanalysis) showed minimal change from baseline: heat RR 1 · 295 vs 1 · 301 (−0 · 5%); cold RR 1 · 275 vs 1 · 271 (+0 · 3%). SARI-adjusted models (influenza/respiratory infection surveillance) produced identical estimates to baseline. These findings suggest residual confounding by air pollution and seasonal infections does not substantially explain our results, though we cannot exclude confounding by unmeasured pollutants or infections not captured by SARI surveillance. **Lag specification:** heat effects were stable across 7–28 day maximum lags; cold effects increased with longer lags (RR 1 · 28 at 7 days to 1 · 78 at 28 days), confirming short-lag models underestimate cold burden. **Degrees of freedom** for the temperature spline (3–5 df) yielded stable results. COVID-19 period exclusion (2020–2021) produced virtually identical estimates. Heatwaves (3 days >P95) showed modest additional effects (RR 1 · 014). Spatial scale comparison showed consistent point estimates between levels with lower heterogeneity at finer resolution (I^2 33% vs 56%).

Period-stratified analysis: The pre-pandemic period (2010–2019) showed heat RR 1 · 15 (95% CI 1 · 11–1 · 20) and cold RR 1 · 11 (95% CI 1 · 08–1 · 13), virtually identical to the pooled estimates. The post-pandemic period (2022–2024) showed heat RR 1 · 18 (95% CI 1 · 13–1 · 23) and cold RR 1 · 07 (95% CI 1 · 04–1 · 10)—remarkably consistent with pre-pandemic estimates. This temporal stability across the COVID-19 pandemic provides strong evidence against substantial survivor bias affecting our findings. **Leave-one-year-out cross-validation** showed stable temporal patterns: heat log-RR ranged from 0 · 41 to 0 · 90 across years (mean 0 · 56, SD 0 · 13), demonstrating consistent effect magnitudes throughout the study period.

Socioeconomic gradient analysis showed that heat effects increased substantially with GDP per capita (Low: RR 0 · 94 [95% CI 0 · 87–1 · 01]; Medium: RR 1 · 19 [95% CI 1 · 11–1 · 27]; High: RR 1 · 48 [95% CI 1 · 32–1 · 67]), likely reflecting urban heat island effects and demographic composition in wealthier, more urbanised areas. Detailed macro-region stratification is presented in Table 7.

6 Discussion

This comprehensive national analysis of 13 · 7 million elderly deaths in Brazil reveals substantial temperature-associated mortality: approximately 61,400 deaths annually (6 · 5% of elderly mortality). Cold-associated deaths exceed heat-associated deaths (2 · 7:1 ratio), reflecting exposure frequency rather than intrinsic lethality.

Three findings merit emphasis. First, heat associations are more plausibly causal: effects are immediate, physiological mechanisms are well-established, and the oldest-old (80+) show heat RR 2 · 04 versus cold RR 1 · 81. Cold associations, while statistically robust, may partly reflect residual seasonal confounding that ecological designs cannot fully address. Second, clear vulnerability gradients identify priority populations for intervention research: the oldest-old (80+), females (33% higher heat-associated mortality), and cardiovascular patients (84% excess on cold days). Third, regional acclimatisation patterns—with heat vulnerability concentrated in cooler southern regions—suggest regionally-tailored approaches.

Under climate change, heat events will increase in frequency and intensity while cold events may decrease, reinforcing the case for heat-focused intervention research. Candidate interventions—requiring evaluation—might include weather warning systems, integration of alerts into chronic disease management, and targeted community health worker outreach.

This study has notable strengths: comprehensive national scope (13 · 7 million deaths over 15 years), methodologically rigorous two-stage DLNM design,[1] 97% model convergence, and comprehensive sensitivity analyses including period-stratified models showing temporal stability across the COVID-19 pandemic.

6.1 Limitations

This ecological time-series design cannot establish causation. Cold associations may partly reflect residual seasonal confounding (infectious disease transmission, behavioural changes, indoor crowding) that is difficult to fully control—the burden estimates should therefore be interpreted as statistical associations rather than preventable deaths. Regional temperature averages cannot capture individual behaviour or indoor modification. COVID-19 survivor bias is a concern, though period-stratified analysis showed remarkable consistency (pre-pandemic heat RR 1 · 15 vs post-pandemic 1 · 18). Extended-lag harvesting estimates were unstable (detailed in Appendix). External causes showed non-null temperature associations (RR ~1 · 15), which may reflect genuine mechanisms (heat impairing cognition and judgment; cold increasing fall risk) rather than pure residual confounding. The 19 excluded non-converged regions represent <2% of the elderly population.

Research priorities include prospective cohort studies with individual-level exposure data, climate projection studies, intervention trials, and equity analyses.

7 Conclusions

Non-optimal temperatures are associated with approximately 61,400 annual elderly deaths in Brazil (6 · 5% of elderly mortality). Cold-associated deaths exceed heat-associated deaths (2 · 7:1 ratio), reflecting exposure frequency rather than per-event danger; however, cold associations may partly reflect residual seasonal confounding, and the burden estimates represent statistical associations rather than directly preventable deaths. Heat associations are more plausibly causal given event-based timing and established physiological mechanisms, and will increase under climate change—warranting prioritisation for intervention research. The oldest-old (80+) and cardiovascular patients show particularly strong associations and represent priority populations.

8 Data sharing

Mortality data are publicly available from DATASUS (http://datasus.saude.gov.br). Temperature data are available from the Copernicus Climate Data Store (https://cds.climate.copernicus.eu). Analysis code will be available at [repository URL] upon publication.

9 Declaration of interests

We declare no competing interests.

10 Acknowledgments

We thank the Brazilian Ministry of Health for maintaining the Mortality Information System (SIM) and DATASUS for data access. We acknowledge the European Centre for Medium-Range Weather Forecasts for the ERA5 reanalysis data.

11 Author contributions

LS: Conceptualisation, methodology, formal analysis, writing (original draft and revision), visualisation. PLS: Conceptualisation, writing (revision and final version).

12 Role of the funding source

No funding received.

13 References

1 Gasparrini A, Guo Y, Hashizume M, *et al.* Mortality risk attributable to high and low ambient temperature: A multicountry observational study. *The Lancet* 2015; **386**: 369–75.

2 Gouveia N, Hajat S, Armstrong B. Socioeconomic differentials in the temperature-mortality relationship in São Paulo, Brazil. *International Journal of Epidemiology* 2003; **32**: 390–7.

3 Son J-Y, Gouveia N, Bravo MA, Freitas CU de, Bell ML. The impact of temperature on mortality in a subtropical city: Effects of cold, heat, and heat waves in São Paulo, Brazil. *International Journal of Biometeorology* 2016; **60**: 113–21.

4 Silveira IH, Oliveira BF de, Cortes TR, Junger WL. The effect of ambient temperature on cardiovascular mortality in 27 brazilian cities. *Science of the Total Environment* 2019; **691**: 996–1004.

5 Aschidamini C, Leon ACMP de. Effect modifiers of the temperature-mortality association for general and older adults population of brazil's metropolitan areas. *Cadernos de Saúde Pública* 2025; **41**: e00042524.

6 Kephart JL, Sánchez BN, Moore JN, *et al.* City-level impact of extreme temperatures and mortality in latin america. *Nature Medicine* 2022; **28**: 1700–5.

7 Masselot P, Mistry M, Vanoli J, *et al.* Excess mortality attributed to heat and cold: A health impact assessment study in 854 cities in europe. *The Lancet Planetary Health* 2023; **7**: e271–81.

8 Schwartz J. Harvesting and long term exposure effects in the relation between air pollution and mortality. *American Journal of Epidemiology* 2005; **161**: 585–94.

9 Zhao Q, Guo Y, Ye T, *et al.* Global, regional, and national burden of mortality associated with non-optimal ambient temperatures from 2000 to 2019: A three-stage modelling study. *The Lancet Planetary Health* 2021; **5**: e415–25.

10 Gasparrini A, Guo Y, Sera F, *et al.* Projections of temperature-related excess mortality under climate change scenarios. *The Lancet Planetary Health* 2017; **1**: e360–7.

11 Bunker A, Wildenhain J, Vandenbergh A, *et al.* Effects of air temperature on climate-sensitive mortality and morbidity outcomes in the elderly; a systematic review and meta-analysis of epidemiological evidence. *EBioMedicine* 2016; **6**: 258–68.

12 Burkart K, Brauer M, Aravkin AY, *et al.* Estimating the cause-specific relative risks of non-optimal temperature on daily mortality: A two-part modelling approach applied to the global burden of disease study. *The Lancet* 2021; **398**: 685–97.

13 Guo Y, Gasparrini A, Armstrong B, *et al.* Global variation in the effects of ambient temperature on mortality: A systematic evaluation. *Epidemiology* 2014; **25**: 781.

14 Instituto Brasileiro de Geografia e Estatística. Censo demográfico 2022: Resultados do universo. 2023.

15 Gasparrini A. Distributed lag linear and non-linear models in r: The package dlnm. *Journal of Statistical Software* 2011; **43**: 1–20.

16 Gasparrini A. Modeling exposure–lag–response associations with distributed lag non-linear models. *Statistics in Medicine* 2014; **33**: 881–99.

17 França E, Abreu DX de, Rao C, Lopez AD. Ill-defined causes of death in brazil: A redistribution method based on the investigation of such causes. *Bulletin of the World Health Organization* 2008; **86**: 39–45.

18 Hersbach H, Bell B, Berrisford P, *et al.* The ERA5 global reanalysis. *Quarterly Journal of the Royal Meteorological Society* 2020; **146**: 1999–2049.

19 Gasparrini A, Armstrong B, Kenward MG. Multivariate meta-analysis for non-linear and other multi-parameter associations. *Statistics in Medicine* 2012; **31**: 3821–39.

20 Tobías A, Armstrong B, Gasparrini A. Mortality on extreme heat days using official thresholds in spain: A multi-city time series analysis. *BMC Public Health* 2017; **17**: 1–8.

21 Gasparrini A, Leone M. Attributable risk from distributed lag models. *BMC Medical Research Methodology* 2014; **14**: 1–8.

22 Zanobetti A, Schwartz J. Mortality displacement in the association of ozone with mortality: An analysis of 48 cities in the united states. *American Journal of Respiratory and Critical Care Medicine* 2008; **177**: 184–9.

23 Armstrong B, Gasparrini A, Tobias A. Models for the relationship between ambient temperature and daily mortality. *Epidemiology* 2017; **28**: e34–6.

24 Hajat S, Vardoulakis S, Heaviside C, Eggen B. Heat-related and cold-related deaths in england and wales: Who is at risk? *Occupational and Environmental Medicine* 2014; **71**: 56–62.

25 Sera F, Armstrong B, Tobias A, *et al.* How urban characteristics affect vulnerability to heat and cold: A multi-country analysis. *International Journal of Epidemiology* 2019; **48**: 1101–12.

26 Analitis A, Katsouyanni K, Biggeri A, *et al.* Effects of cold weather on mortality: Results from 15 european cities within the PHEWE project. *American Journal of Epidemiology* 2008; **168**: 1397–408.

27 Keatinge WR, Coleshaw SR, Easton JC, Cotter F, Mattock MB, Chelliah R. Increased platelet and red cell counts, blood viscosity, and plasma cholesterol levels during heat stress, and mortality from coronary and cerebral thrombosis. *The American Journal of Medicine* 1986; **81**: 795–800.

28 Clegg A, Young J, Iliffe S, Rikkert MO, Rockwood K. Frailty in elderly people. *The Lancet* 2013; **381**: 752–62.

14 Tables

Table 1: Temperature-mortality associations at intermediate and immediate spatial levels

Metric	Intermediate (n=129 regions)	Immediate (n=495 regions)
Model performance		
Total regions	133	510
Converged models	129 (97 · 0%)	495 (97 · 1%)
Region-days	660,980	2,302,539
Total deaths analysed	13,677,712	13,677,712
Minimum mortality temperature		
MMT (°C)	25 · 01	24 · 76
Extreme temperature effects (vs MMT)		
Heat P99 (28 · 7°C) RR (95% CI)	1 · 238 (1 · 186–1 · 292)	1 · 183 (1 · 157–1 · 209)
Heat P99 95% prediction interval	0 · 92–1 · 66	0 · 98–1 · 43
Cold P1 (20 · 2°C/18 · 7°C) RR (95% CI)	1 · 101 (1 · 078–1 · 126)	1 · 099 (1 · 084–1 · 115)
Cold P1 95% prediction interval	0 · 89–1 · 36	0 · 95–1 · 27
Moderate temperature effects		
Heat P95 RR (95% CI)	1 · 011 (0 · 994–1 · 028)	0 · 989 (0 · 978–0 · 999)
Cold P5 RR (95% CI)	1 · 052 (1 · 040–1 · 064)	1 · 047 (1 · 041–1 · 053)
Heterogeneity		
I^2 (%)	55 · 6	33 · 2
Cochran's Q (df)	4,617 (2,048)	11,836 (7,904)

Metric	Intermediate (n=129 regions)	Immediate (n=495 regions)
Q p-value	$<0 \cdot 001$	$<0 \cdot 001$
Interpretation	Moderate	Low-moderate

RR=relative risk. MMT=minimum mortality temperature. CI=confidence interval (uncertainty in pooled estimate); PI=prediction interval (expected range of effects in a new region, accounting for between-region heterogeneity). PIs are substantially wider than CIs when $I^2>0$, reflecting true variation in temperature-mortality associations across regions.

Table 2: Temperature-attributable mortality burden and years of life lost

Metric	Intermediate level	Immediate level
15-year totals (2010–2024)		
Total deaths analysed	13,677,712	13,677,712
Heat-attributable deaths (AN)	244,207 (182,086–307,560)	231,284 (190,721–271,051)
Cold-attributable deaths (AN)	650,985 (541,070–768,292)	471,211 (406,735–531,772)
Total attributable deaths	895,192 (800,741–987,756)	702,495 (636,406–763,109)
Attributable fractions		
Heat AF (%)	1 · 79 (1 · 33–2 · 25)	1 · 69 (1 · 39–1 · 98)
Cold AF (%)	4 · 76 (3 · 96–5 · 62)	3 · 45 (2 · 97–3 · 89)
Total AF (%)	6 · 54 (5 · 85–7 · 22)	5 · 14 (4 · 65–5 · 58)
Annual averages		
Heat deaths/year	16,738 (12,480–21,080)	18,711 (15,429–21,928)
Cold deaths/year	44,618 (37,084–52,658)	38,121 (32,905–43,021)
Total deaths/year	61,356 (54,882–67,700)	56,832 (51,486–61,736)
Cold:heat ratio	2 · 67:1	2 · 04:1
Years of life lost		
Total YLL (15 years)	11,467,000	8,998,000
Annual YLL	786,000	728,000
YLL heat/year	214,000	240,000
YLL cold/year	572,000	488,000
YLL rate (per 100,000 elderly)	2,446	2,267
YLL per attributable death	12 · 81 years	12 · 81 years
Burden sensitivity scenarios (intermediate)		
Excluding 2020–2021 (pandemic)†	~850,000	—
Pollution-adjusted RR curves‡	~885,000 (−1%)	—
SARI-adjusted RR curves§	~895,000 (±0%)	—

AN=attributable number. AF=attributable fraction. YLL=years of life lost. All burden estimates with 95% CIs from Monte Carlo simulation (N=1,000). †Estimated by applying period-specific mortality to same RR curves; COVID-19 exclusion showed virtually identical RR estimates. ‡Based on pollution-adjusted RRs: heat 1 · 295 (−0 · 5%), cold 1 · 275 (+0 · 3%); net burden change approximately −1% due to heat reduction partially offset by cold increase. §SARI-adjusted RRs were identical to baseline. Note: YLL estimates represent an upper bound assuming each attributable death loses the full age-specific life expectancy; if

heat deaths are substantially displaced (harvesting), actual life-years lost per death may be considerably shorter—potentially days to weeks for severely frail individuals.

Table 3: Effect modification by age group

Age group	Heat RR (95% CI)	Cold RR (95% CI)	I^2 (%)	Converged
Intermediate level (133 regions)				
60–69 years	1 · 23 (1 · 16–1 · 30)	1 · 38 (1 · 29–1 · 46)	2 · 0	129/133
70–79 years	1 · 42 (1 · 33–1 · 51)	1 · 41 (1 · 31–1 · 53)	20 · 4	129/133
80+ years	2 · 04 (1 · 80–2 · 31)	1 · 81 (1 · 69–1 · 94)	22 · 2	129/133
Immediate level (510 regions)				
60–69 years	1 · 09 (1 · 04–1 · 13)	1 · 11 (1 · 07–1 · 16)	3 · 9	495/510
70–79 years	1 · 22 (1 · 17–1 · 26)	1 · 14 (1 · 09–1 · 19)	10 · 7	495/510
80+ years	1 · 55 (1 · 46–1 · 63)	1 · 36 (1 · 31–1 · 41)	16 · 7	495/510

Age gradient (80+ vs 60–69):

- Intermediate: Heat +66%, Cold +31%
- Immediate: Heat +42%, Cold +23%

Table 4: Effect modification by sex and cause of death

Stratum	Heat RR (95% CI)	Cold RR (95% CI)	I^2 (%)
Sex—Intermediate level			
Male	1 · 46 (1 · 37–1 · 56)	1 · 62 (1 · 51–1 · 73)	5 · 4
Female	1 · 94 (1 · 73–2 · 16)	1 · 50 (1 · 42–1 · 60)	14 · 5
Female vs Male difference	+33%***	−7% (NS)	
Sex—Immediate level			
Male	1 · 28 (1 · 24–1 · 33)	1 · 29 (1 · 24–1 · 34)	5 · 2
Female	1 · 53 (1 · 45–1 · 60)	1 · 24 (1 · 20–1 · 28)	11 · 7
Female vs Male difference	+19%***	−4% (NS)	
Cause—Intermediate level			
Cardiovascular (I00–I99)	1 · 47 (1 · 37–1 · 58)	1 · 84 (1 · 70–1 · 99)	7 · 5
Respiratory (J00–J99)	1 · 63 (1 · 47–1 · 82)	1 · 42 (1 · 30–1 · 56)	15 · 7
External (V01–Y98)	1 · 15 (1 · 05–1 · 26)	1 · 15 (0 · 99–1 · 33)	6 · 3
Other causes	1 · 67 (1 · 51–1 · 84)	1 · 44 (1 · 36–1 · 53)	25 · 2
Cause—Immediate level			
Cardiovascular	1 · 22 (1 · 17–1 · 27)	1 · 24 (1 · 19–1 · 30)	0 · 04
Respiratory	1 · 29 (1 · 21–1 · 37)	1 · 27 (1 · 18–1 · 36)	18 · 7
External	0 · 99 (0 · 84–1 · 18)	1 · 15 (0 · 99–1 · 34)	0 · 0
Other	1 · 39 (1 · 33–1 · 45)	1 · 20 (1 · 16–1 · 25)	17 · 2

***p<0 · 001; NS=not statistically significant (p>0 · 05).

Table 5: Meta-regression—regional effect modifiers

Moderator	Heat p-value	Cold p-value	Significant?
Intermediate level (n=129)			
Urbanisation rate	$0 \cdot 100$	$0 \cdot 001$	Cold only
GDP per capita	$0 \cdot 187$	$0 \cdot 071$	Neither
Elderly proportion (%)	$0 \cdot 001$	$<0 \cdot 001$	Both
Temperature variability (SD)	$<0 \cdot 001$	$<0 \cdot 001$	Both
Immediate level (n=493)			
Urbanisation rate	$<0 \cdot 001$	$<0 \cdot 001$	Both
GDP per capita	$0 \cdot 001$	$<0 \cdot 001$	Both
Elderly proportion (%)	$<0 \cdot 001$	$<0 \cdot 001$	Both
Temperature variability (SD)	$<0 \cdot 001$	$<0 \cdot 001$	Both

Direction of effects (Intermediate level):

- Higher elderly proportion → Higher heat vulnerability (slope=$0 \cdot 05$) and cold vulnerability (slope=$0 \cdot 07$)
- Higher temperature variability → Higher heat risk (slope=$0 \cdot 06$) and cold risk (slope=$0 \cdot 08$)
- Higher urbanisation → Lower cold risk (urban heat island protection)

Table 6: Sensitivity analyses

Analysis	Heat RR (95% CI)	Cold RR (95% CI)	Change from baseline
Confounding adjustment—Intermediate level			
Baseline (dry-bulb temperature)	1 · 301 (1 · 259–1 · 344)	1 · 271 (1 · 239–1 · 303)	Reference
+ PM . and O (CAMS satellite)	1 · 295 (1 · 253–1 · 338)	1 · 275 (1 · 243–1 · 308)	Heat −0 · 5%; Cold +0 · 3%
+ SARI (respiratory infections)	1 · 301 (1 · 259–1 · 344)	1 · 271 (1 · 239–1 · 303)	Heat ±0%; Cold ±0%
+ Both (fully adjusted)	1 · 295 (1 · 253–1 · 338)	1 · 275 (1 · 243–1 · 308)	Heat −0 · 5%; Cold +0 · 3%
Lag structure—Intermediate level			
7 days	1 · 71 (1 · 58–1 · 84)	1 · 28 (1 · 23–1 · 32)	—
14 days	1 · 77 (1 · 62–1 · 94)	1 · 52 (1 · 44–1 · 60)	—
21 days (baseline)	1 · 76 (1 · 60–1 · 93)	1 · 62 (1 · 53–1 · 72)	—
28 days	1 · 70 (1 · 55–1 · 87)	1 · 78 (1 · 66–1 · 90)	—
Lag structure—Immediate level			
7 days	1 · 55 (1 · 50–1 · 61)	1 · 16 (1 · 14–1 · 18)	—
14 days	1 · 57 (1 · 51–1 · 63)	1 · 28 (1 · 25–1 · 31)	—
21 days (baseline)	1 · 58 (1 · 51–1 · 65)	1 · 34 (1 · 30–1 · 38)	—
28 days	1 · 56 (1 · 48–1 · 63)	1 · 46 (1 · 41–1 · 51)	—
Heatwave effects			
Intermediate (3 days >P95)	1 · 014 (1 · 006–1 · 021)	—	—
Immediate (3 days >P95)	1 · 007 (1 · 001–1 · 013)	—	—
Spatial comparison			
Intermediate (133 regions)	1 · 238 (1 · 186–1 · 292)	1 · 101 (1 · 078–1 · 126)	—
Immediate (510 regions)	1 · 183 (1 · 157–1 · 209)	1 · 099 (1 · 084–1 · 115)	−4 · 4% heat; −0 · 2% cold

CAMS=Copernicus Atmosphere Monitoring Service. SARI=severe acute respiratory infection (SIVEP-Gripe surveillance). Confounding adjustment models fitted on 97 intermediate regions with complete covariate data; baseline RRs in this section (1 · 301/1 · 271) differ from main pooled estimates (1 · 238/1 · 101 in Table 1)

because they derive from this restricted sample with complete pollution and SARI data, enabling direct comparison of adjusted vs unadjusted models on identical observations.

Table 7: Supplementary analyses—Macro-region stratification and socioeconomic gradients

Stratum	N regions	Heat RR (95% CI)	Cold RR (95% CI)	Mean temp (°C)
By macro-region				
South	18	1 · 67 (1 · 42–1 · 96)	0 · 96 (0 · 91–1 · 01)	19 · 3
Southeast	33	1 · 37 (1 · 27–1 · 48)	1 · 05 (1 · 02–1 · 08)	22 · 7
Central-West	15	1 · 17 (1 · 10–1 · 23)	1 · 09 (1 · 02–1 · 15)	24 · 3
North	21	0 · 94 (0 · 87–1 · 01)	1 · 01 (0 · 82–1 · 24)	25 · 7
Northeast	42	0 · 96 (0 · 89–1 · 04)	1 · 36 (1 · 21–1 · 52)	26 · 3
By GDP tertile				
Low	46	0 · 94 (0 · 87–1 · 01)	1 · 08 (0 · 96–1 · 22)	—
Medium	43	1 · 19 (1 · 11–1 · 27)	1 · 11 (1 · 07–1 · 16)	—
High	40	1 · 48 (1 · 32–1 · 67)	1 · 02 (1 · 00–1 · 05)	—
By urbanisation tertile				
Low	47	0 · 94 (0 · 87–1 · 01)	1 · 15 (1 · 05–1 · 25)	—
Medium	44	1 · 33 (1 · 21–1 · 46)	1 · 05 (1 · 00–1 · 09)	—
High	38	1 · 26 (1 · 19–1 · 32)	1 · 07 (1 · 04–1 · 09)	—

Macro-region results show a clear climate-adapted gradient: heat effects strongest in cooler regions (South), cold effects strongest in warmer regions (Northeast). Socioeconomic gradients show larger heat effects in higher-GDP, more urbanised regions, consistent with urban heat island effects. All analyses at intermediate level. N regions indicates number of regions converging in the second-stage meta-analysis.

15 Figures

Figure 1: Pooled exposure-response relationship between temperature and elderly mortality

The J-shaped curve shows relative risk of mortality across the temperature distribution, with the minimum mortality temperature (MMT) at $25 \cdot 0$°C as reference. Both cold (left) and heat (right) extremes are associated with increased mortality. Shading represents 95% confidence intervals.

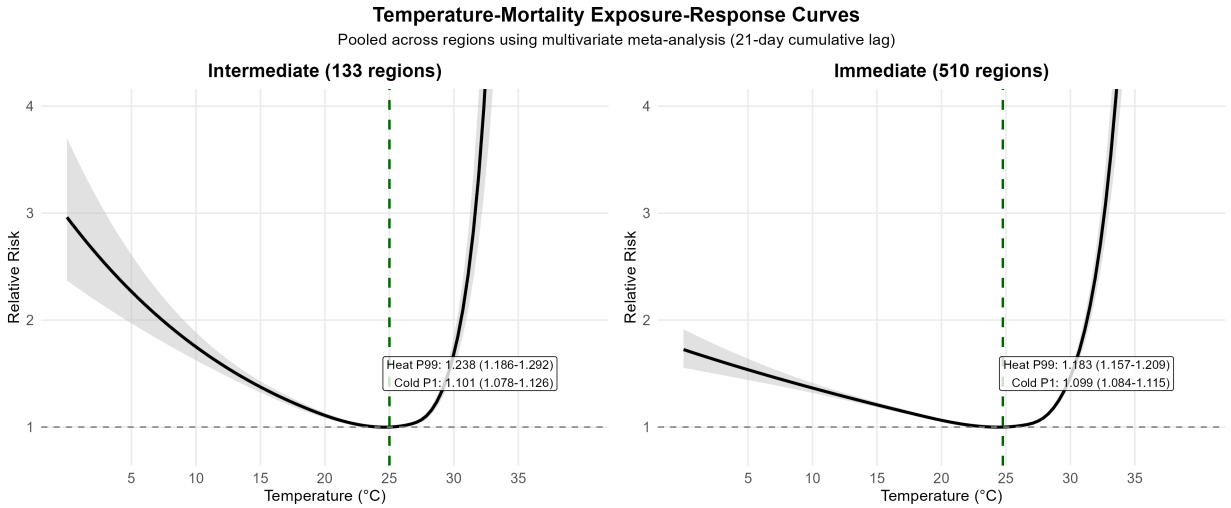

Figure 2: Effect modification by age group

Temperature-mortality associations stratified by age (60–69, 70–79, 80+ years). The oldest-old (80+) show the highest vulnerability to both heat and cold extremes, with heat RR $2 \cdot 04$ and cold RR $1 \cdot 81$.

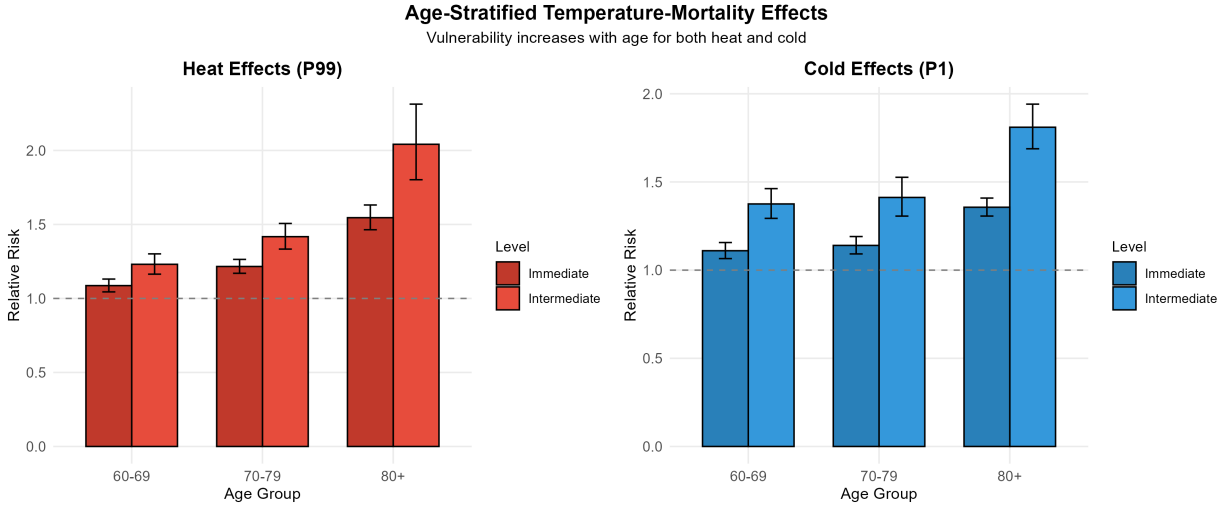

Figure 3: Effect modification by sex

Temperature-mortality associations stratified by sex. Females show 33% higher heat vulnerability than males ($p<0 \cdot 001$); males show slightly higher cold vulnerability (not statistically significant).

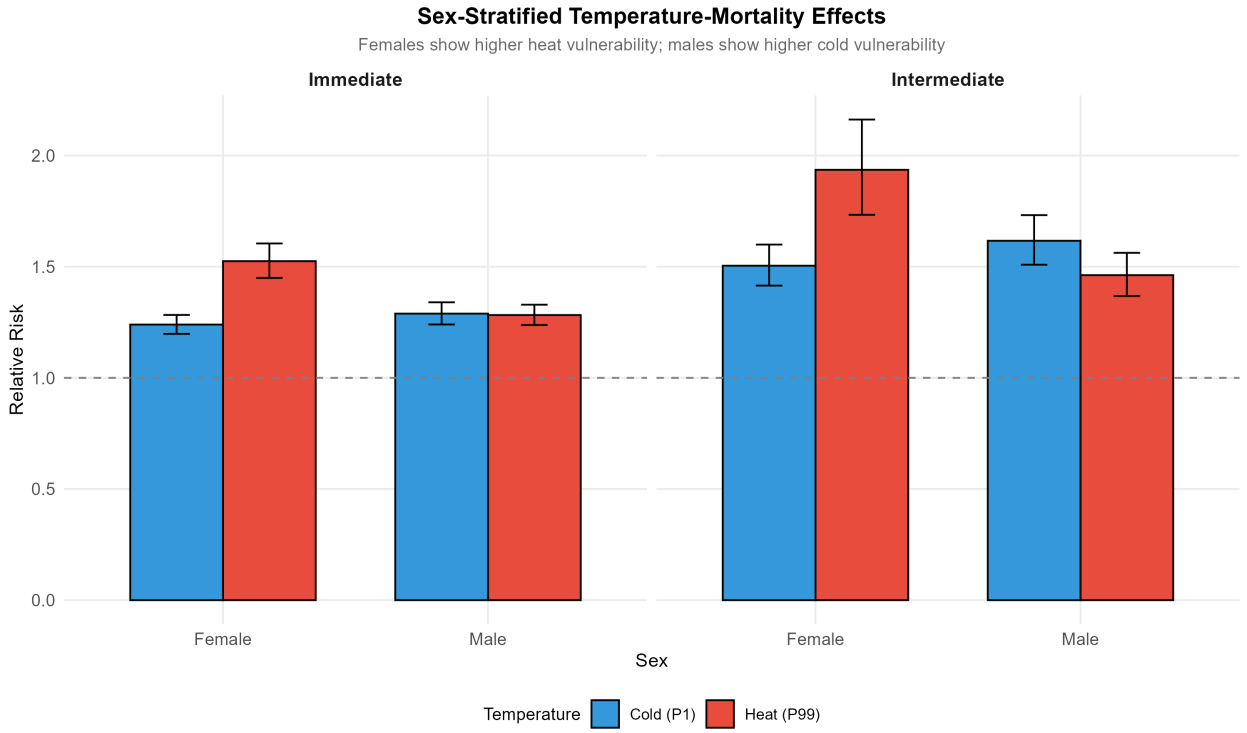

Figure 4: Effect modification by cause of death

Temperature-mortality associations stratified by cause. Cardiovascular deaths show the strongest cold association (RR 1 · 84, 84% excess). Respiratory deaths show elevated effects for both extremes. External causes show modest associations (RR ~1 · 15), which may reflect genuine mechanisms rather than pure confounding (see Appendix).

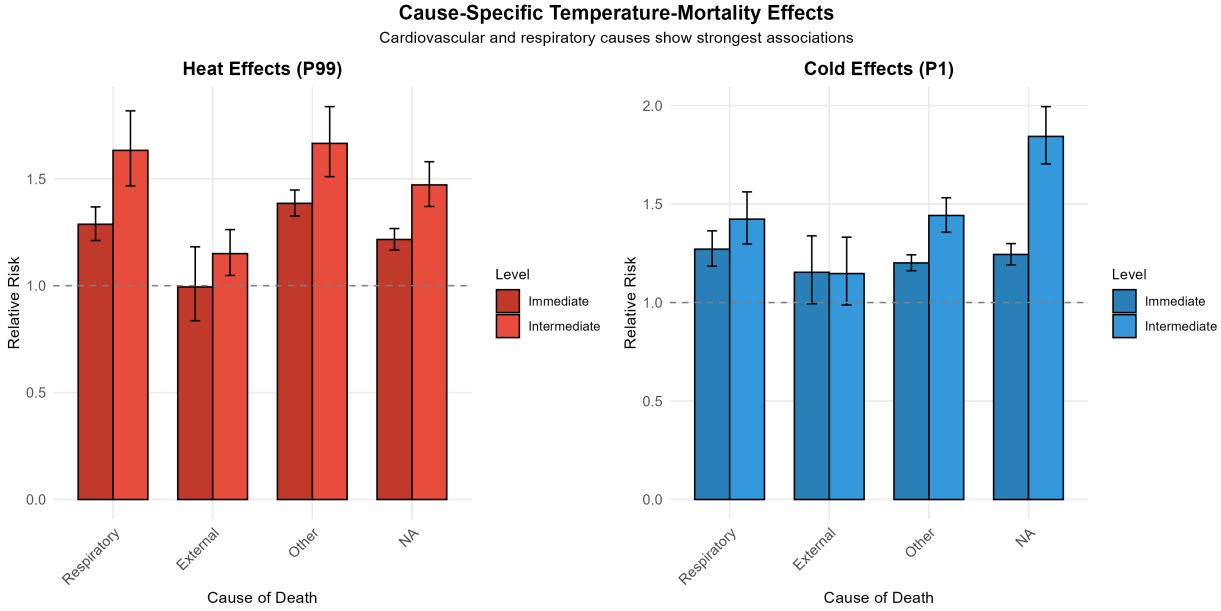

Figure 5: Geographic distribution of heat effects across Brazil

Spatial variation in heat-attributable mortality (RR at P99) across 133 intermediate regions. Higher values (warmer colours) indicate greater heat vulnerability.

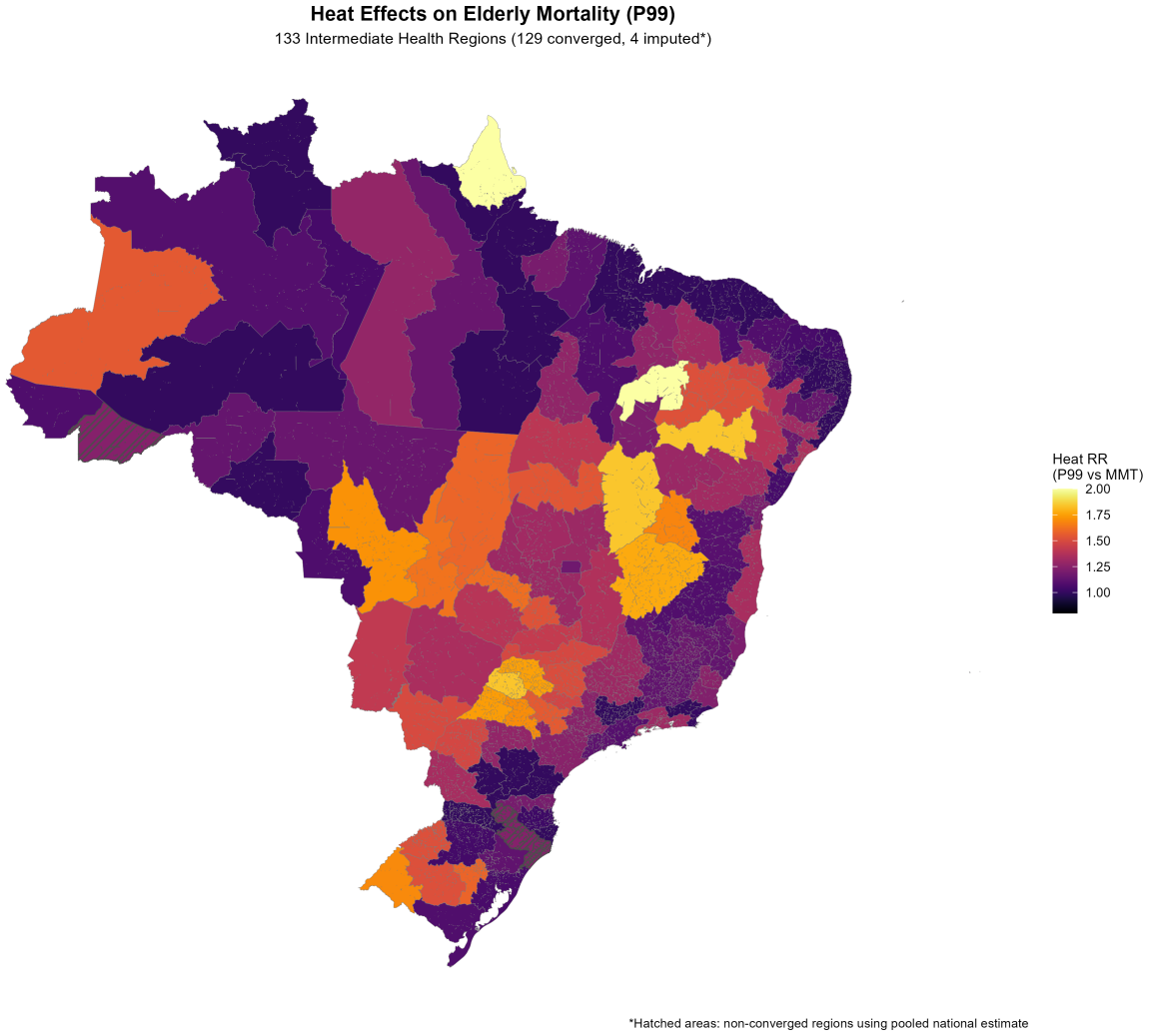

Figure 6: Geographic distribution of cold effects across Brazil

Spatial variation in cold-attributable mortality (RR at P1) across 133 intermediate regions. Southern and highland regions show highest cold vulnerability.

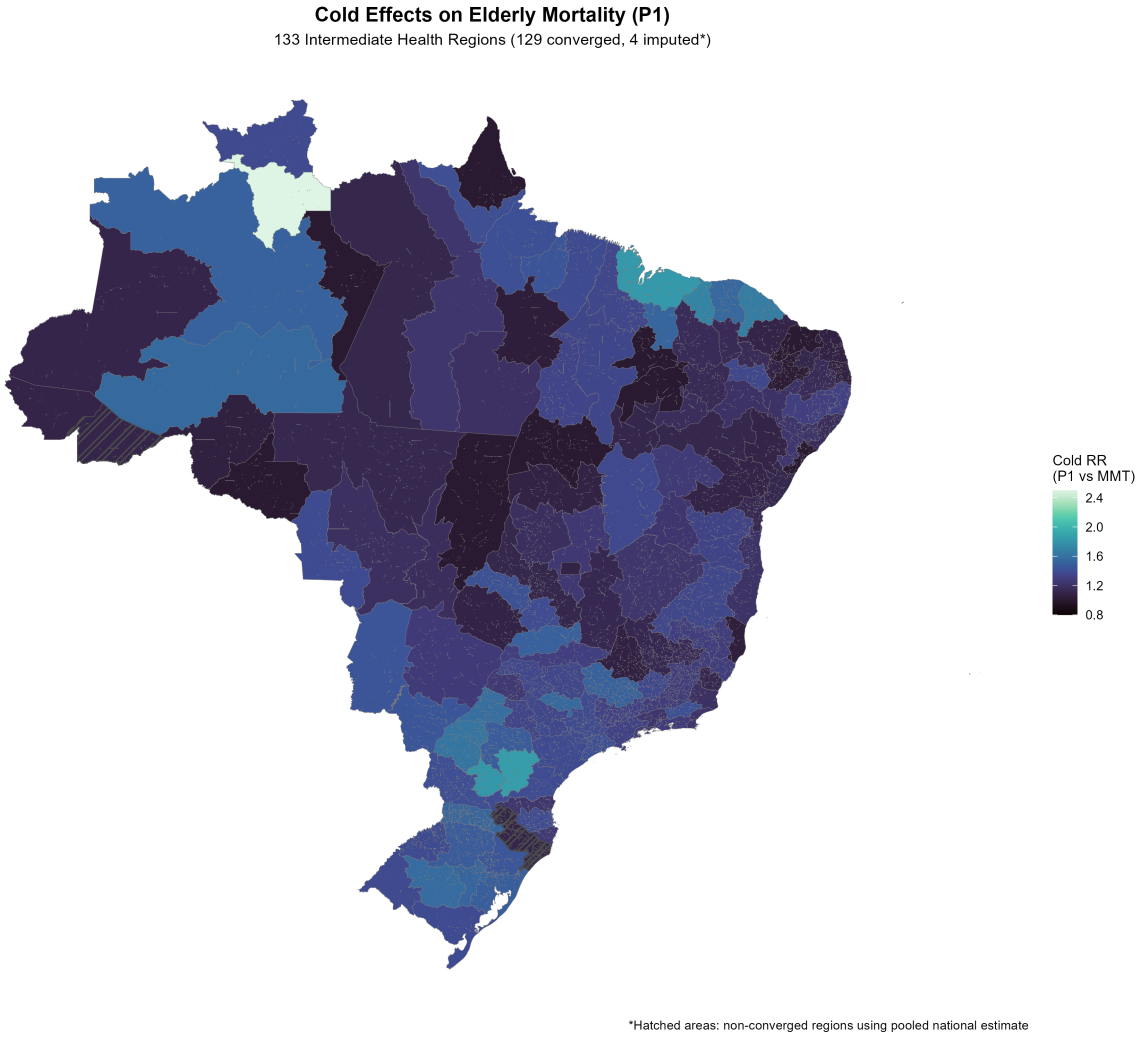

16 Appendix

16.1 Appendix Table A1: DLNM model specification

Parameter	Specification
Outcome	Daily death count (quasi-Poisson)
Exposure	Daily mean 2m temperature (°C)
Cross-basis: Exposure dimension	Natural cubic spline, 4 df
Knots (internal)	P10 ($18 \cdot 6$°C), P75 ($26 \cdot 6$°C), P90 ($27 \cdot 8$°C)
Boundary knots	0°C, 40°C
Cross-basis: Lag dimension	Natural cubic spline, 4 df
Maximum lag	21 days
Lag knots	Equal intervals on log scale
Confounders	
Time trend/seasonality	Natural spline, 8 df per year
Day of week	Indicator variables (7 levels)
Public holidays	Indicator variable
Offset	log(elderly population)
Meta-analysis	
Method	Multivariate random-effects
Estimation	Restricted maximum likelihood (REML)

16.2 Appendix Table A2: Temperature distribution

Percentile	Temperature (°C)	Interpretation
P1	$18 \cdot 7$–$20 \cdot 2$	Extreme cold threshold
P$2 \cdot 5$	~19	Cold definition for burden
P5	~20	Moderate cold
P25	~22	Lower quartile
P50	~24	Median
P75	~26	Upper quartile
P95	~28	Moderate heat
P$97 \cdot 5$	~29	Heat definition for burden
P99	$28 \cdot 7$	Extreme heat threshold

16.3 Appendix Figure A1: Temperature distribution across study regions

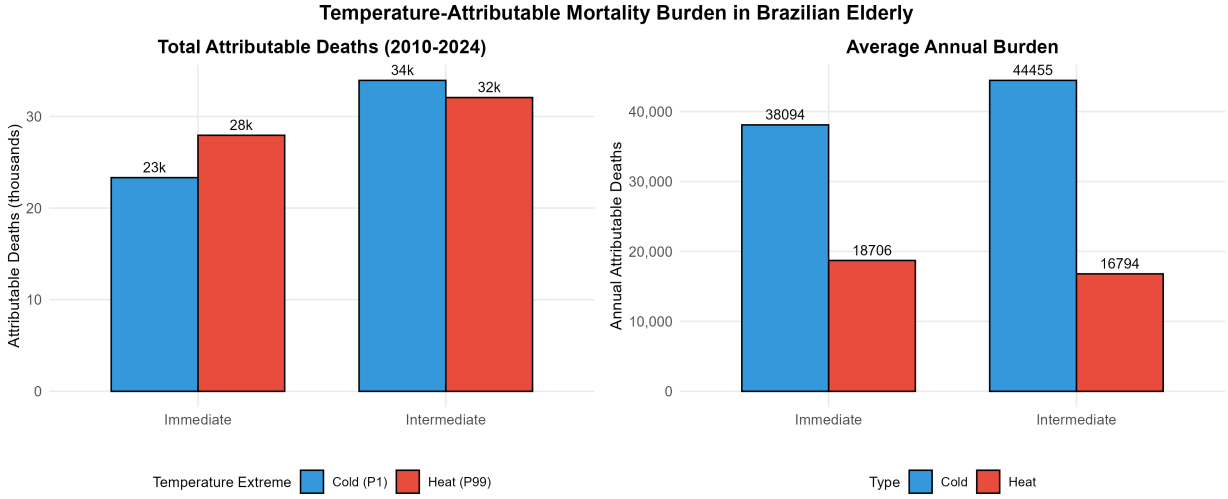

16.4 Appendix Figure A2: Seasonal patterns in mortality and temperature

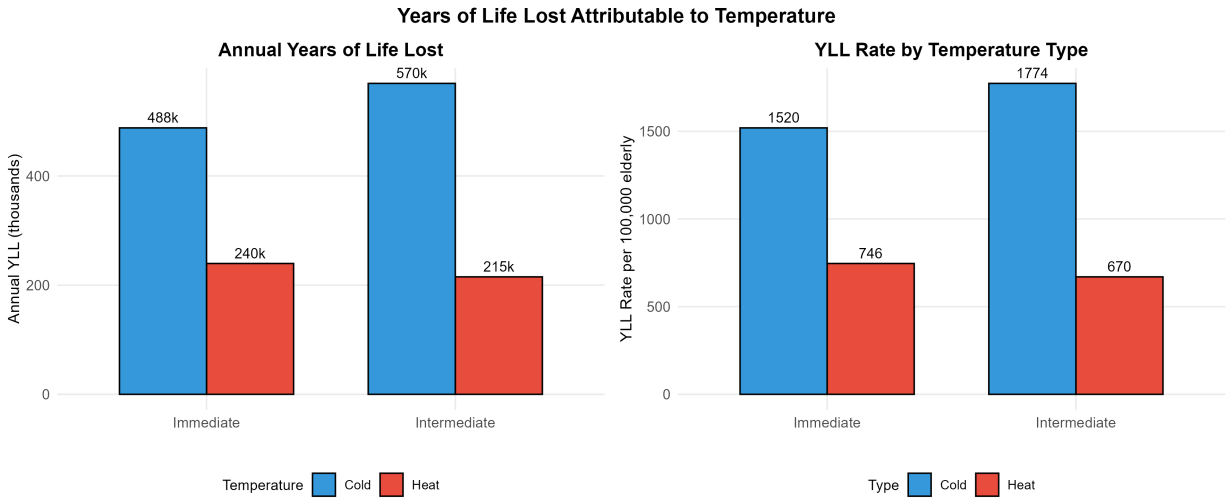

16.5 Appendix Figure A3: Lag-response structure for heat and cold

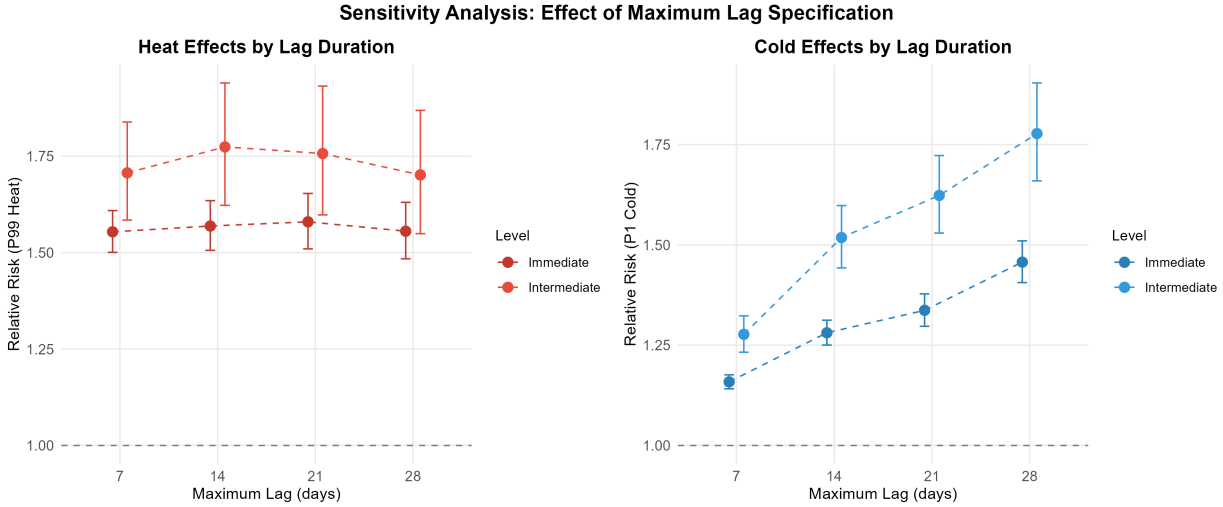

16.6 Appendix Table A3: Regions excluded due to non-convergence

Regions were excluded from the meta-analysis when first-stage DLNM models failed to converge, typically due to sparse mortality data or insufficient temperature variation. The 97% convergence rate (129/133 intermediate, 495/510 immediate) is consistent with comparable multi-region temperature-mortality studies.

Code	Region name	Level	State	Deaths/day	Low-death days	Temp spread	Likely cause
1201	Rio Branco	Inter.	AC	8 · 2	0 · 4%	6 · 5°C	Low temp variance
4202	Criciúma	Inter.	SC	17 · 1	0 · 0%	10 · 9°C	Model specification
4203	Lages	Inter.	SC	7 · 7	0 · 7%	18 · 2°C	Model specification
4205	Caçador	Inter.	SC	4 · 1	8 · 0%	18 · 2°C	Low deaths
110004	Ji-Paraná	Immed.	RO	4 · 7	5 · 9%	10 · 7°C	Low deaths
120002	Cruzeiro do Sul	Immed.	AC	1 · 5	62 · 3%	6 · 5°C	Sparse data
310053	Frutal	Immed.	MG	4 · 3	7 · 3%	11 · 8°C	Low deaths
410003	Paranavaí	Immed.	PR	3 · 6	12 · 0%	17 · 2°C	Sparse data
410004	Maringá	Immed.	PR	6 · 7	1 · 1%	17 · 1°C	Model specification
410010	Londrina	Immed.	PR	5 · 0	4 · 8%	18 · 2°C	Model specification
410029	Campo Mourão	Immed.	PR	3 · 2	16 · 7%	17 · 0°C	Sparse data
420003	Joinville	Immed.	SC	6 · 3	1 · 7%	10 · 7°C	Model specification
420005	Lages	Immed.	SC	6 · 2	2 · 1%	18 · 2°C	Model specification
420006	São Joaquim	Immed.	SC	1 · 9	43 · 7%	18 · 1°C	Sparse data
420008	Curitibanos	Immed.	SC	3 · 3	15 · 3%	18 · 8°C	Sparse data
420014	Canoinhas	Immed.	SC	2 · 2	37 · 2%	18 · 0°C	Sparse data
420015	São Bento do Sul	Immed.	SC	2 · 5	29 · 6%	18 · 4°C	Sparse data

Code	Region name	Level	State	Deaths/day	Low-death days	Temp spread	Likely cause
420017	Jaraguá do Sul	Immed.	SC	4 · 8	4 · 9%	17 · 6°C	Low deaths
430039	Vacaria	Immed.	RS	2 · 5	28 · 1%	19 · 2°C	Sparse data

Inter.=intermediate level. Immed.=immediate level. State abbreviations: AC=Acre, MG=Minas Gerais, PR=Paraná, RO=Rondônia, RS=Rio Grande do Sul, SC=Santa Catarina. Low-death days = percentage of days with 1 death. Temp spread = difference between 99th and 1st temperature percentiles. Regions with <5 mean deaths/day or >10% low-death days typically lack statistical power for non-linear DLNM estimation. Region names are based on the principal city within each geographic region.

16.7 Appendix: Frailty-adjusted YLL scenario

Our main YLL estimates (~786,000 annually) assume temperature-vulnerable individuals have the same remaining life expectancy as the general elderly population—an implausible assumption. This appendix presents an illustrative frailty-adjusted scenario to bound the uncertainty.

Rationale for 70% reduction assumption: Temperature-attributable deaths are concentrated among individuals with cardiovascular disease, respiratory conditions, and clinical frailty—not healthy elderly. Clegg et al. (2013) documented that elderly individuals with moderate-to-severe frailty (Clinical Frailty Scale 6–7) have median survival of 2–4 years, compared to 10+ years for robust age-matched peers.[28] We selected 70% as an illustrative—not empirically derived—reduction factor representing a plausible mid-range scenario.

Explicit calculation:

Step 1: Unadjusted YLL (upper bound)

- Annual attributable deaths: 61,356
- Mean remaining life expectancy (Brazilian life tables, age 60+): 12 · 8 years
- Unadjusted annual YLL: 61,356 × 12 · 8 = **785,357 786,000**

Step 2: Frailty-adjusted YLL (illustrative scenario)

- Assumption: Temperature-vulnerable individuals have 70% shorter remaining life expectancy than population average
- Frailty-adjusted life expectancy: 12 · 8 × (1 − 0 · 70) = 12 · 8 × 0 · 30 = **3 · 84 3 · 8 years**
- Frailty-adjusted annual YLL: 61,356 × 3 · 8 = **233,153 240,000**
- Reduction: (786,000 − 240,000) / 786,000 = **69 · 5% 70%**

Step 3: Summary table

Scenario	Life expectancy	Annual YLL	% of upper bound	Interpretation
Unadjusted (population life tables)	12 · 8 years	~786,000	100%	Upper bound
70% frailty adjustment (illustrative)	3 · 8 years	~240,000	31%	Plausible mid-range
Severe frailty + pure harvesting	Days–weeks	Near zero	~0%	Lower bound for displaced deaths

Important caveats: The 70% reduction is illustrative, not empirically calibrated to Brazilian temperature-mortality data. The true reduction depends on: (a) the actual frailty distribution among temperature-attributable deaths; (b) the proportion representing pure harvesting vs. additional mortality; (c) cause-

specific patterns (cardiovascular deaths may involve more vs. less frail individuals than respiratory deaths). This scenario demonstrates the sensitivity of YLL estimates to frailty assumptions rather than providing a definitive adjusted estimate.

Interpretation: The "true" YLL lies between these bounds. Without individual-level frailty data, we cannot determine its precise location. The unadjusted estimate overstates the life-years at stake; the frailty-adjusted estimate may be more realistic for policy interpretation. Even the lower bound does not eliminate the rationale for intervention, as displaced deaths involve suffering, healthcare costs, and family burden not captured by life-year metrics.

16.8 Appendix: Extended harvesting analysis

We assessed whether temperature deaths represent true excess mortality or displacement of imminent deaths by comparing cumulative effects at extended lags (7–35 days). **This analysis is exploratory and cannot reliably quantify displacement magnitude due to substantial statistical uncertainty.**

Appendix Table A4: Harvesting analysis—cumulative heat effects at extended lags (intermediate level only)

Lag horizon	Cumulative RR	95% CI	ERR (%)	Interpretation
7 days	1 · 49	1 · 23–1 · 80	+49 · 0	Initial effect (significant)
14 days	1 · 46	1 · 08–1 · 95	+46 · 0	Minimal attenuation
21 days	1 · 17	0 · 84–1 · 63	+17 · 0	Substantial attenuation (CI crosses unity)
28 days	1 · 08	0 · 72–1 · 62	+8 · 0	Near-null effect (wide CI)
35 days	1 · 00	0 · 67–1 · 50	0 · 0	Complete attenuation

RR=relative risk. ERR=excess relative risk (RR−1, expressed as percentage). CI=confidence interval. I^2 heterogeneity remained extremely high (98–99%) across all horizons, reflecting substantial variation in temperature-mortality dynamics across Brazilian regions. Cold harvesting estimates showed implausible patterns at intermediate horizons (RR < 1 at 21–28 days) and are not reported due to numerical instability.

Appendix Figure A4: Harvesting analysis—cumulative effects at extended lags

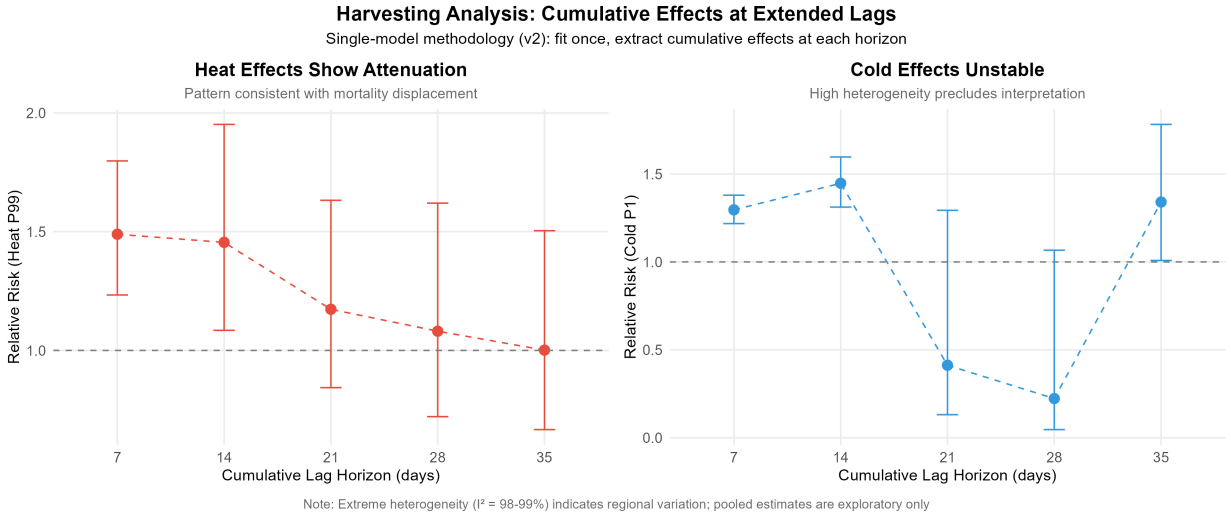

Note: This figure shows exploratory results with substantial uncertainty. Confidence intervals overlap across all lag horizons, precluding reliable conclusions about displacement magnitude. The apparent attenuation of heat effects at longer lags is suggestive but not statistically demonstrable.

Heat harvesting: Heat effects showed substantial attenuation at longer lags (cumulative RR declining from 1 · 49 at 7 days to 1 · 00 at 35 days), a pattern consistent with near-complete displacement. The initial 7-day effect was statistically significant (95% CI 1 · 23–1 · 80), but significance was lost by 21 days as confidence intervals crossed unity (CI 0 · 84–1 · 63). The harvesting ratio of ~100% suggests that heat-associated deaths largely represent displacement of deaths that would have occurred within weeks regardless.

Caveats: Despite this suggestive pattern, three factors preclude definitive conclusions: (1) I^2 heterogeneity remained extremely high (98–99% across all horizons), indicating that pooled estimates mask substantial regional variation; (2) confidence intervals overlap substantially across lag horizons; (3) the extreme heterogeneity suggests the harvesting ratio varies widely across Brazilian regions and should not be interpreted as a single national parameter.

Cold harvesting: Cold-exposure harvesting estimates were uninformative. The pattern was implausible (RR declining to <1 at intermediate horizons before recovering at 35 days), likely reflecting methodological instability rather than biological phenomena. These are not reported.

Immediate-level exclusion: The immediate-level harvesting analysis is not reported due to computational constraints at the finest spatial resolution.

Interpretation: The declining ERR from +49% at 7 days to 0% at 35 days suggests substantial mortality displacement, consistent with heat primarily affecting already-frail individuals. However, extreme heterogeneity (I^2 = 98–99%) means this pattern varies dramatically across regions. These exploratory findings are hypothesis-generating only. Critically, even displaced deaths involve suffering and healthcare utilisation, making heat prevention valuable regardless of displacement magnitude.

16.9 Appendix: Meta-regression details

Given the moderate to substantial heterogeneity observed across regions (I^2 = 55 · 6% at intermediate level), we used multivariate meta-regression to identify regional characteristics that explained variation in temperature-mortality associations.

Temperature variability: The standard deviation of daily temperature emerged as the strongest modifier. Regions with higher variability showed significantly higher vulnerability to both heat (coefficient = 0 · 08, 95% CI 0 · 05–0 · 11; p<0 · 001) and cold (coefficient = 0 · 06, 95% CI 0 · 03–0 · 09; p<0 · 001). This is consistent with acclimatisation theory: populations in stable climates are adapted to narrow ranges.

Elderly population proportion: Each percentage point increase in elderly proportion was associated with 5% higher heat effects (p=0 · 001) and 7% higher cold effects (p<0 · 001), suggesting demographic ageing will compound climate change risks.

Urbanisation: For cold effects, higher urbanisation was associated with *lower* mortality effects (coefficient = −0 · 03, 95% CI −0 · 05 to −0 · 01; p=0 · 001), likely reflecting urban heat island protection. Heat effects showed inconsistent patterns across spatial scales.

GDP per capita: No significant association at intermediate level (p>0 · 28), but significant at immediate level (p<0 · 001), suggesting economic factors operate at finer spatial resolutions.

Model fit: Including these moderators explained 34% of between-region heterogeneity for heat (residual I^2 36 · 7%) and 28% for cold (residual I^2 40 · 0%). Substantial unexplained heterogeneity remains, likely reflecting local healthcare quality, housing, air conditioning prevalence, and behavioural adaptations.

16.10 Appendix: Cause-of-death analysis

Cardiovascular deaths (ICD-10 I00–I99): Showed the highest cold vulnerability: RR 1 · 84 (95% CI 1 · 70–1 · 99), representing 84% excess mortality on cold days. This is consistent with cold-cardiovascular pathways: sympathetic activation, vasoconstriction, increased blood pressure and viscosity, and platelet activation favouring thrombosis. Heat effects were substantial but lower: RR 1 · 47 (95% CI 1 · 37–1 · 58).

Respiratory deaths (ICD-10 J00–J99): Elevated vulnerability to both extremes: heat RR $1 \cdot 63$ (95% CI $1 \cdot 47$–$1 \cdot 82$), cold RR $1 \cdot 42$ (95% CI $1 \cdot 30$–$1 \cdot 56$), consistent with the respiratory system's direct exposure to inspired air.

External causes (ICD-10 V01–Y98): External causes were included as a contrast outcome to help assess the specificity of temperature-mortality associations. The observed RR $\sim 1 \cdot 15$ for external causes has two plausible explanations:

Genuine mechanisms: Heat may impair cognitive function and judgment, increase alcohol consumption and associated accidents, and increase outdoor activity exposure to hazards.[24] Cold may increase fall risk (particularly on wet surfaces in southern Brazil), cause hypothermia deaths coded as external causes, and trigger cardiovascular events during physical exertion that are misclassified.

Residual confounding: The association may reflect unmeasured seasonal factors not fully captured by temporal adjustment.

Given these alternative explanations, using external causes to calibrate primary estimates (e.g., dividing cardiovascular RR by $1 \cdot 15$) is methodologically problematic. We therefore do not attempt quantitative calibration. The key observation for validity assessment is *proportionality*: external cause effects (RR $1 \cdot 15$) are substantially smaller than cardiovascular (RR $1 \cdot 84$) or respiratory (RR $1 \cdot 42$) effects, suggesting that if residual confounding explains part of primary estimates, it likely explains only a modest fraction rather than the majority of observed associations.